OXFORD

Journal of Petrology, 2023, **64**, 1–19
https://doi.org/10.1093/petrology/egad085
Advance access publication date 1 December 2023
Original Manuscript

The Systematics of Olivine CaO + Cr-Spinel in High-Mg# Arc Volcanic Rocks: Evidence for in-Situ Mantle Wedge Depletion at the Arc Volcanic Front

Susanne M. Straub [1,*], Valentina Batanova[2], Alexander Sobolev[2], Arturo Gómez-Tuena[3], Ramon Espinasa-Perena[4], W. Lindsey Fleming[5], Ilya N Bindeman[6], Finlay M. Stuart[7] and Elisabeth Widom[8] and Yoshiyuki Iizuka[9]

[1]Lamont Doherty Earth Observatory at the Columbia University, 61 Route 9W, Palisades NY 10964, USA
[2]Univ. Grenoble Alpes, Univ. Savoie Mont Blanc, CNRS, IRD, Univ. Gustave Eiffel, ISTerre , 38000 Grenoble, France
[3]Instituto de Geología, Universidad Nacional Autónoma de México, Cd. Universitaria, Coyoacán 04510, Mexico City, México
[4]Instituto de Geologia, Investigación Científica, Copilco Universidad, Coyoacán, 04360 Ciudad de México, CDMX, Mexico
[5]Freie Universität Berlin, Institut für Geologische Wissenschaften, Berlin, Germany
[6]Department of Earth Sciences, University of Oregon, Eugene, OR, 97403-1272, USA
[7]Isotope Geosciences Unit, Scottish Universities Research and Reactor Centre, East Kilbride G75 0QF, UK
[8]Department of Geology and Environmental Earth Science, Miami University, 118 Shideler Hall, 250 S. Patterson Ave, Oxford OH 45056, USA
[9]Institute of Earth Sciences, Academia Sinica, 128 Academia Road, Sec. 2, Nangang, Taipei 11529, Taiwan, ROC

*Corresponding author. Phone: +845 365 8464, Fax: +845 365 8155. E-mail: smstraub@ldeo.columbia.edu

We investigated the state of the arc background mantle (i.e. mantle wedge without slab component) by means of olivine CaO and its Cr-spinel inclusions in a series of high-Mg# volcanic rocks from the Quaternary Trans-Mexican Volcanic Belt. Olivine CaO was paired with the Cr# [molar Cr/(Cr + Al) ∗100] of Cr-spinel inclusions, and 337 olivine+Cr-spinel pairs were obtained from 33 calc-alkaline, high-K and OIB-type arc front volcanic rocks, and three monogenetic rear-arc basalts that lack subduction signatures. Olivine+Cr-spinels display coherent elemental and He–O isotopic systematics that contrast with the compositional diversity of the bulk rocks. All arc front olivines have low CaO (0.135 ± 0.029 wt %) relative to rear-arc olivines which have the higher CaO (0.248 ± 0.028 wt %) of olivines from mid-ocean ridge basalts. Olivine $^{3}He/^{4}He$–$\delta^{18}O$ isotope systematics confirm that the olivine+Cr-spinels are not, or negligibly, affected by crustal basement contamination, and thus preserve compositional characteristics of primary arc magmas. Variations in melt H_2O contents in the arc front series and the decoupling of olivine CaO and Ni are inconsistent with controls on the olivine CaO by melt water and/or secondary mantle pyroxenites. Instead, we propose that low olivine CaO reflects the typical low melt CaO of high-Mg# arc magmas erupting through thick crust. We interpret the inverse correlation of olivine CaO and Cr-spinel Cr# over a broad range of Cr# (∼10–70) as co-variations of CaO, Al and Cr of their (near) primary host melts, which derived from a mantle that has been variably depleted by slab-flux driven serial melt extraction. Our results obviate the need for advecting depleted residual mantle from rear- and back-arc region, but do not upset the larger underlying global variations of melt CaO high-Mg# arc magmas worldwide, despite leading to considerable regional variations of melt CaO at the arc front of the Trans-Mexican Volcanic Belt.

Key words: chromian spinel; olivine; magnesian andesite; subduction; mantle

INTRODUCTION

Forsteritic olivines and their Cr-spinel inclusions ('olivine+Cr-spinels' hereafter) crystallize first in many primitive magmas. Because olivine+Cr-spinels are stable over only a narrow temperature interval and are sensitive to melt composition (Dick & Bullen, 1984; Clynne & Borg, 1997; Sobolev *et al.*, 2007), they can capture compositional characteristics of primitive mantle melts. Several studies discussed how magmatic olivine+Cr-spinels may track mantle composition and processes (Dick & Bullen, 1984; Clynne & Borg, 1997; Nekrylov *et al.*, 2018). The Cr# [=molar Cr/(Cr + Al) ∗100] of magmatic Cr-spinels has been used as indicator of mantle source depletion (e.g. Dick & Bullen, 1984; Clynne & Borg, 1997; Kamenetsky *et al.*, 2001; Nekrylov *et al.*, 2018), in similar ways as the Cr# range of residual Cr-spinels in mantle rocks is used as indicator of residual mantle fertility (e.g. Dick & Bullen, 1984; Warren, 2016; Pearce & Reagan, 2019; Pearce & Arculus, 2021). The olivine Fo [=molar ratio of Mg/(Mg + Fe)∗100] has long been used as proxy to the Mg# [=molar Mg/(Mg + Fe^{2+}) ∗100] of their equilibrium melts (Roeder & Emslie, 1970; Putirka, 2008). Moreover, olivine trace elements have been used to test for the presence of peridotitic versus pyroxenitic lithologies in the source of oceanic intraplate and arc magmas (e.g. Sobolev *et al.*, 2005; Sobolev *et al.*, 2007; Straub *et al.*, 2008; Straub *et al.*, 2011; Díaz-Bravo *et al.*, 2014; Søager *et al.*, 2015; Brandt *et al.*, 2017; Zamboni *et al.*, 2017; Rasmussen *et al.*, 2020). While interpretation of what mantle source characteristics are captured by the olivine trace elements remains controversial (Kamenetsky *et al.*, 2001; Matzen *et al.*, 2013; Matzen *et al.*, 2017; Nekrylov *et al.*, 2018), the potential clearly exists. The use of olivine+Cr-spinels as tracers of mantle source characteristics is particularly attractive in arc magmas, where melt hybridization is common (e.g. Eichelberger, 1978; Kent *et al.*, 2010) and where olivine+Cr-spinels antecrysts may be the only

Received: March 17, 2023. **Revised:** November 20, 2023. **Accepted:** November 26, 2023

way to assess the source characteristics of in-mixed mafic melts that became absorbed into the larger volumes of co-existing silicic magma bodies (e.g. Nixon, 1988; Straub & Martin-Del Pozzo, 2001; Sas *et al.*, 2017; Leeman & Smith, 2018).

In this study, we focus on the CaO contents of forsteritic olivines from the continental Trans-Mexican Volcanic Belt (TMVB), which are evaluated together with the Cr-spinel inclusions. As high-level trace element in olivine, CaO has been extensively measured in olivines from mid-ocean ridge basalts (MORB), from intraplate basalts (Sobolev *et al.*, 2007) and from arc magmas (Clynne & Borg, 1997; Kamenetsky *et al.*, 2006; Bryant *et al.*, 2011; Tamura *et al.*, 2011; Díaz-Bravo *et al.*, 2014; Søager *et al.*, 2015; Ammannati *et al.*, 2016; Gavrilenko *et al.*, 2016; Brandt *et al.*, 2017; Zamboni *et al.*, 2017; Nekrylov *et al.*, 2018; Mesa & Lange, 2021). It became clear that CaO is more variable in arc olivines, and can be similar to or higher or lower than in MORB olivines. However, a consistent feature of arc olivines is that their CaO concentrations in continental arc magmas (e.g. Trans-Mexican Volcanic Belt, Aeolian arc, Andean Southern Volcanic Zone, the Cascades, Kamchatka and Costa Rica) are collectively lower than those of MORB olivines. At first view, the low olivine CaO may simply reflect the typical low melt CaO of continental arc magmas (Plank & Langmuir, 1988; Turner & Langmuir, 2015), given that CaO as incompatible element in olivine with low olivine/melt partition coefficient (Kd^{Ca}_{oliv}) of ~0.02 depends on the melt CaO (Jurewicz & Watson, 1988; Laubier *et al.*, 2014; Ma & Shaw, 2021). However, there are other factors. For one, it has been argued that the Kd^{Ca}_{oliv}—and thus the olivine CaO - is lowered by the elevated melt water of hydrous arc magmas (Feig *et al.*, 2006; Gavrilenko *et al.*, 2016; Mesa & Lange, 2021). Furthermore, it has been proposed that the low olivine CaO reflects an increased CaO retention in source by secondary pyroxenites (Herzberg, 2006; Díaz-Bravo *et al.*, 2014; Søager *et al.*, 2015).

In order to evaluate the causes of the low CaO contents of olivines in continental arc magmas, we present new high-precision data of olivine CaO and their Cr-spinel inclusions in forsteritic olivines from the continental Trans-Mexican Volcanic Belt (TMVB). In the TMVB, olivine+Cr-spinels are often the only phenocrysts in the monogenetic basalts to andesites, and in the basaltic andesites and andesites of the composite volcanoes. They are antecrysts in the dacites magmas of composite volcanoes (Nixon, 1988; Straub & Martin-Del Pozzo, 2001; Schaaf *et al.*, 2005). The new olivine+Cr-spinel data were obtained from a previously well-characterized set of olivine-phyric volcanic rocks, which includes several monogenetic volcanoes of the Sierra Chichinautzin Volcanic Field and of the Serdán basin, as well as composite volcano Popocatépetl. In addition, we analyzed for the first time olivine+Cr-spinels in monogenetic rear-arc basalts that are free from subduction influence and thus serve as proxy to the TMVB mantle wedge prior to subduction modifications (Luhr, 1997; Díaz-Bravo *et al.*, 2014; Gómez-Tuena *et al.*, 2014). Many of the arc front olivines are 'high-Ni olivines' which are olivines with a higher Ni at a given Fo than possible for olivines in partial melts of peridotite mantle, e.g. MORB olivines (Sobolev *et al.*, 2005) and that have been linked to secondary pyroxenite in the TMVB mantle wedge (Straub *et al.*, 2008; Straub *et al.*, 2011). This allows for testing the proposed link between mantle pyroxenites and low olivine CaO, while the systematic differences in melt water content of the TMVB magma series investigated (Cervantes & Wallace, 2003*a*; Cervantes & Wallace, 2003*b*; Johnson *et al.*, 2009; Roberge *et al.*, 2009) allows for evaluating the influence of melt water on olivine CaO.

GEOLOGICAL BACKGROUND

The Trans-Mexican Volcanic Belt

The Trans-Mexican Volcanic Belt is an active Quaternary volcanic arc linked to the subduction of the Cocos and Rivera plates along the Middle American Trench (Figure 1). Detailed reviews on its evolution and magmatic series can be found elsewhere (e.g. Gómez-Tuena *et al.*, 2018*b*) and only pertinent facts are reiterated here. The TMVB has a broad, irregular arc front marked by nine composite volcanoes and several monogenetic fields, which are constructed on a continental crustal basement that varies in age (Proterozoic to Cenozoic), composition and thickness (~35–50 km). The composite volcanoes erupted several hundreds of km^3 of calc-alkaline andesitic and dacitic magmas, which display the arc-typical enrichments of large-ion lithophile elements (LILE) relative to high-field strength elements (HSFE) and rare earth elements (REE). The numerous small-volume (usually $<<1$ km^3) cones and lava flows of the monogenetic fields are much more diverse in composition (e.g. Siebe *et al.*, 2004*a*; Siebe *et al.*, 2005; Gómez-Tuena *et al.*, 2018*b*; Larrea *et al.*, 2019). Calc-alkaline basaltic andesites are most abundant, but next to andesites and dacites, high-MgO basalts (up to 10 wt % MgO; Mg# ≤72) and rare rhyolites also occur (Supplementary Appendix Figure S1). A compositionally striking subgroup consists of K-rich basalts and basaltic andesites which are enriched in light REE and have the steep heavy REE patterns indicative of garnet-bearing residues (Luhr *et al.*, 1989; Lange & Carmichael, 1990; Gómez-Tuena *et al.*, 2018*b*) (Supplementary Appendix Figure S2). Another notable monogenetic variety is the so-called 'OIB-type' arc front magmas, which have the enriched, and only weakly fractionated trace element patterns of intraplate magmas (e.g. Wallace & Carmichael, 1999; Schaaf *et al.*, 2005). The OIB-type volcanics have been considered to best approximate background mantle melts (Wallace & Carmichael, 1999; Cervantes & Wallace, 2003*b*; Johnson *et al.*, 2009; Gómez-Tuena *et al.*, 2018*b*), but they also have been linked to locally enriched mantle domains that may (Straub *et al.*, 2013*a*; Straub *et al.*, 2015) or may not (Turner *et al.*, 2017; Turner & Langmuir, 2022) be related to slab recycling in the active subduction regime.

In the monogenetic fields, the diverse arc front magma types can be closely associated both temporally and spatially. For example, in the Sierra Chichinautzin Volcanic Field (Figure 1), late Pleistocene calc-alkaline, OIB-type and K-rich series erupted within a few 1000 years and within a few kilometers of one another and sometimes even from the same vent (Siebe *et al.*, 2004*a*; Siebe *et al.*, 2005; Straub *et al.*, 2014; Straub *et al.*, 2015). Comprehensive geochemical studies of bulk rock major and trace elements and Sr–Nd–Pb–Hf isotope ratios, complemented by olivine He–O isotopes and composition, demonstrate that the compositional diversity originates from a mantle source that has been made heterogeneous by the slab flux and melt extraction (Wallace & Carmichael, 1999; Straub *et al.*, 2008; Johnson *et al.*, 2009; Straub *et al.*, 2011; Straub *et al.*, 2015; Ahmadi *et al.*, 2023).

Rationale for sample and site selection

We selected olivine+Cr-spinels from 36 high-Mg# basalts to dacites. The Mg# numbers [=molar ratio $Mg/(Mg+Fe^{2+})*100$] of the bulk rocks range between 50 and 73, and most (>87%) have Mg# > 60 (Figure 1; Supplementary Appendix Figure S1). As typical for the high-Mg# TMVB magmas, olivine+Cr-spinels are the only, or dominant phenocrysts in the monogenetic basalts to andesites (Siebe *et al.*, 2004*a*; Schaaf *et al.*, 2005; Straub *et al.*, 2011; Straub *et al.*, 2013*a*; Straub *et al.*, 2014). Rare high-Mg# orthopyroxenes

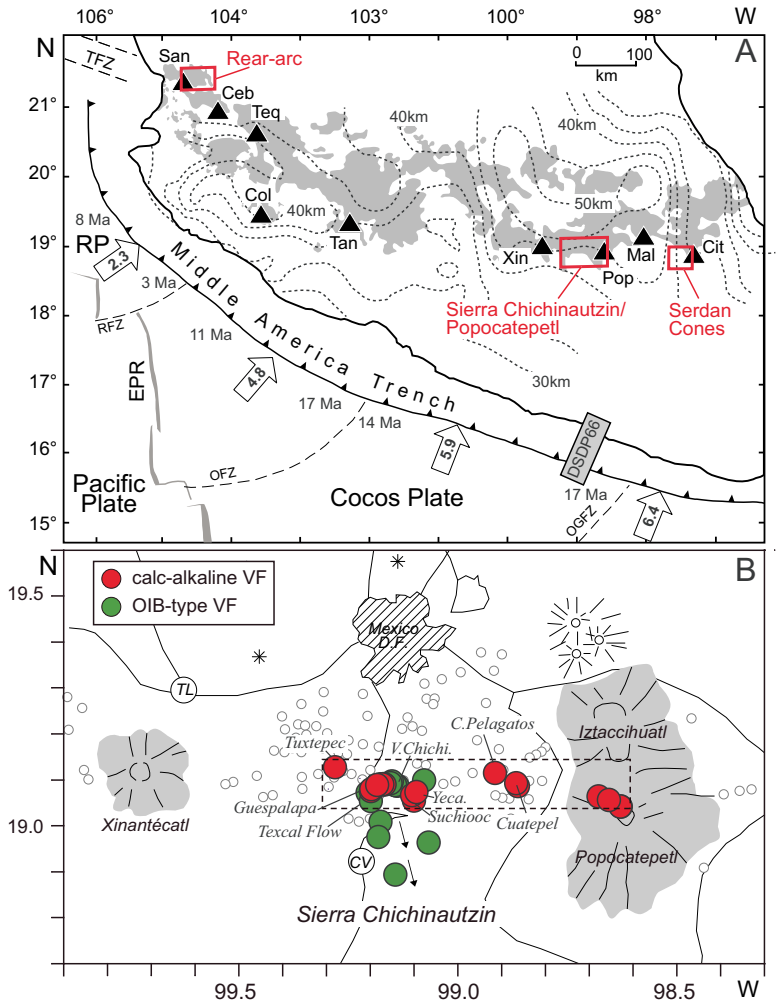

Fig. 1. Map of the Trans-Mexican Volcanic Belt **a:** Trans-Mexican Volcanic Belt (*grey shaded*) with 9 Quaternary composite volcanoes (*black triangles*) Sangangüey (San), Ceboruco (Ceb), Tequila (Teq), Colima (Col), Tancítaro (Tan), Xinantécatl (Xin; also Nevado de Toluca), Popocatépetl (Pop), Malinche (Mal), Citlaltépetl (Cit; also Pico de Orizaba). *Red rectangles* denote the three study areas (Rear-arc; Sierra Chichinautzin/ Popocatépetl; Serdan Cones). Crustal thickness contours *(stippled)* beneath TMVB, convergence rate in cm/yr (*arrows with enclosed numbers*) and age (Ma) of subducting Rivera Plate (RP) and Cocos Plate are from Gómez-Tuena *et al.* (2018*b*). EPR, East Pacific Rise; RFZ, Rivera Fracture Zone; OFZ, Orozco Fracture Zone; OGFZ, O'Gorman Fracture Zone. **b:** Close-up of Sierra Chichinautzin Volcanic Field/Popocatépetl study area with monogenetic volcanoes (open small grey circles) of the Sierra Chichinautzin Volcanic Field and adjacent composite volcanoes Xinantécatl and Popocatépetl-Iztaccihuatl. *Colored filled circles*—sample locations. *Stippled rectangle* (ca. 10 × 70 km) denotes zone of volcanic vents which can produce 10- to 20-km-long lavas flowing (*arrow*) downhill to the south. *Italic names*—monogenetic volcanoes sampled: *V. Chichi.*, Volcan Chichinautzin; *Yeca.*, Yecahuazac.; CV, City of Cuernavaca; TL, City of Toluca.

have been observed in same monogenetic basalts and andesites (Straub *et al.*, 2014), and plagioclase phenocrysts appear in the most silica-rich OIB-type varieties. Clinopyroxene phenocrysts are absent, which is typical for the TMVB high-Mg# mafic magmas (e.g. Blatter & Carmichael, 2001). At Popocatépetl, olivine+Cr-spinels are the only phenocrysts in basaltic andesites and mafic andesites, and they occur as antecrysts in the plagioclase- and pyroxene-phyric Popocatépetl dacites (e.g. Straub *et al.*, 2008; Straub *et al.*, 2011).

Thirty-one samples are from ten different monogenetic volcanoes; five samples are from composite volcano Popocatépetl. Despite their small size, several of the monogenetic volcanoes (e.g. Texcal Flow, V. Chichinautzin, Suchiooc, Cuatepel) are composed of two and more compositionally distinct lava flows (e.g. Siebe *et al.*, 2004*a*; Straub *et al.*, 2013*a*; Straub *et al.*, 2014). An important criterion for sample selection was the lack of consanguinity for most of the 36 samples, which means they are not related to each other by fractional crystallization and/or varying extents of partial melting. The lack of consanguinity was determined on the basis of the metadata, for example by the distinct Sr-Nd-Pb-Hf isotope ratios or distinct incompatible trace element patterns at a similar high bulk rock Mg# of the sample. According to these criteria, 31 of the samples represent distinct melt batches from distinct mantle sources (e.g. Straub *et al.*, 2011; Straub *et al.*, 2013*a*; Díaz-Bravo *et al.*, 2014; Gómez-Tuena *et al.*, 2014; Straub *et al.*, 2014; Straub *et al.*, 2015). The samples selected are from three study areas (Figure 1):

Arc front: Sierra Chichinautzin/Popocatépetl

The principal study area between 99.3° and 98.4°W includes Popocatépetl and several monogenetic volcanoes in the Sierra Chichinautzin Volcanic Field to the west (marked Sierra Chichinautzin/Popocatépetl in Fig 1). All volcanic vents are located within a narrow, arc front-parallel corridor of ~10 km width and ~70 km length, from which individual lavas extend up to ~20 km downhill to the south (Wallace & Carmichael, 1999; Siebe *et al.*, 2004*a*; Agustín-Flores *et al.*, 2011; Straub *et al.*, 2013*a*; Straub *et al.*, 2014; Straub *et al.*, 2015). The Quaternary arc volcanoes are presumably

constructed on Paleozoic high-grade metamorphic complexes of the Mixteco terrane (Gómez-Tuena *et al.*, 2007; Ortega-Gutiérrez *et al.*, 2008; Gómez-Tuena *et al.*, 2018*b*). Subduction parameters such as distance to trench, height above slab (~100 km), slab dip and crustal thickness (~45 km) are all similar, thus do not account for differences in melt composition, which include calc-alkaline, high-K and OIB-type magmas. Calc-alkaline magmas are basaltic andesites, andesites and dacites from Popocatépetl, and basalts, basaltic andesites and andesites from the monogenetic volcanoes V. Cuatepel, Cerro Pelagatos, Guespalapa Volcanic Complex and the Suchiooc Cone. High-K basaltic andesites were collected from V. Tuxtepec and Yecahuazac Cone. OIB-type basalts and basaltic andesites were collected from V. Chichinautzin, Texcal Flow, and the Suchiooc lava flows. Many of monogenetic volcanoes are constructed by several, compositional distinct lavas flows and/or pyroclastic cones; and sometimes the chronology of their events can be reconstructed (e.g. Siebe *et al.*, 2004*a*; Straub *et al.*, 2013*a*; Straub *et al.*, 2014).

Arc front: Serdán Basin

The 'Serdán basalts' are located ~122 km east of Popocatépetl in the western foothills of the Citlaltepetl and Sierra Negra volcanoes. They are calc-alkaline, high-MgO (~8.2–9.4 wt %), high-Mg# (~68.5–71) basalts and basaltic andesites that have enriched Sr–Nd–Pb–Hf isotope signatures (LaGatta, 2003), which have been linked to either basement contamination (Cai *et al.*, 2014) or to recycling of tectonically eroded fore-arc crust (Parolari *et al.*, 2021). The Serdán basalts erupt ~150 km above slab through the ~35–40 km thick continental crust of possibly Precambrian age (Gómez-Tuena *et al.*, 2018*b*). Three studied Serdán basalts are from three cones near the town of Serdán (Cerro Resbaladero, Western and Eastern Mesa Techachales); a forth sample (SM18) was taken from an unnamed basaltic andesite flow ca. 15 km to the south.

Rear-arc: Monogenetic volcanoes near Sangangüey

The 'rear-arc basalts' (n = 4) are high-TiO_2 monogenetic basalts that erupted within ~10–20 km of the calc-alkaline Sangangüey composite volcano at 104.7°W (Gómez-Tuena *et al.*, 2014). Their incompatible trace element patterns lack subduction signatures and resemble those of oceanic alkali basalts. Rear-arc olivines have Ni and CaO concentrations comparable to those in mid-ocean ridge basalts (MORB) (Díaz-Bravo *et al.*, 2014; Gómez-Tuena *et al.*, 2014). Erupting ~320 km above slab, rear-arc basalts represent melts from a TMVB mantle not modified by the slab flux. The continental basement near Sangangüey is not older than late Triassic (Cavazos-Tovar *et al.*, 2020) and is estimated to be ~40 km thick (Gómez-Tuena *et al.*, 2018*b*).

MATERIALS AND METHODS

A sample overview, details of sample preparation, analytical methods and all new analytical data are given in the Supplementary Appendix 1 and in the Supplementary Appendix Tables 1 to 7. We report new electron microprobe (EMP) data of olivine CaO and their Cr-spinel inclusions for all 36 TMVB samples. The olivine composition was measured with two different beam currents of 100 and 900 nA, respectively. All 100 = nA data for olivine CaO are new, whereas their major element oxides and Ni data have been reported previously except for the eight samples denoted in Supplementary Appendix Table (Straub *et al.*, 2008; Straub *et al.*, 2011; Straub *et al.*, 2013*a*; Straub *et al.*, 2014; Straub *et al.*, 2015). All 900 nA EMP data are new.

In order to obtain a characteristic olivine signature for each sample, we first analyzed ~10 to 20 olivine phenocrysts per sample, including core-to-rim transects with a 100-nA beam current (see Supplementary Appendix Table 5). This helped to determine the dominant olivine population for a given sample. On the basis of the '100 nA' data, representative Cr-spinel-bearing olivine crystals were selected for re-analysis with a 900-nA beam (olivine), and for Cr-spinel analysis. This two-step process ensures the comparability of the microbeam data with the $^3He/^4He$ and $\delta^{18}O$ data obtained from handpicked olivine crystals.

In order to obtain olivine+Cr-spinel pairs, ~2 to 4 olivine points were measured with a 900-nA beam around a Cr-spinel inclusion which was analyzed 1 or 2 times. A total of 337 olivine-spinel pairs were obtained from 246 individual olivine phenocrysts (some phenocrysts have multiple pairs). The olivine+Cr-spinel pairs are mostly from calc-alkaline volcanic rocks (n = 184 pairs), followed by OIB-type (n = 105), high-K (n = 31) and rear-arc (n = 17) magmas. Since the high-K and calc-alkaline samples have many similar compositional characteristic, the two high-K samples are included in the calc-alkaline series for clarity in text and figures (but not in the table), except when clearly different. For clarity, only the 900-nA EMP data are displayed the figures; analytical errors of these data are always smaller than symbol size.

For most of the 36 samples, metadata already existed, which are bulk rock major and trace elements and Sr-Nd-Pb-Hf isotope ratios and olivine He–O isotopes (LaGatta, 2003; Straub *et al.*, 2008; Straub *et al.*, 2011; Straub *et al.*, 2013*a*; Cai *et al.*, 2014; Díaz-Bravo *et al.*, 2014; Gómez-Tuena *et al.*, 2014; Straub *et al.*, 2014; Straub *et al.*, 2015). In order to complete the metadata for all samples studied, we obtained additional olivine $^3He/^4He$ and olivine $\delta^{18}O$ data for 10 samples, as well as additional bulk rock major and trace element data for five samples. Previous and new bulk rock data are compiled in their entirety in Supplementary Appendix Table 1.

RESULTS

Olivine major element and He–O isotope composition

The additional new olivine data confirm our prior results (Straub *et al.*, 2008; Straub *et al.*, 2011; Straub *et al.*, 2013*a*). As previously, the average olivine Fo per sample, which ranges from Fo78 to Fo90, plots mostly in, or close to, equilibrium with the bulk rock Mg#'s (Figure 2a) (see Supplementary Appendix Table 1 and Figure S3 and S4 for the calculation of bulk rock ferric Fe). Thus, most olivines can be linked to the bulk rock composition by means of their Fo content (Straub *et al.*, 2008; Straub *et al.*, 2011; Straub *et al.*, 2013*a*). An obvious exception is the forsteritic (up to Fo = 91.2) olivine+Cr-spinels antecrysts in the Popocatépetl dacites (SiO_2 = 65 wt %; Mg# =62), which plot well off the equilibrium line.

The additional olivine $^3He/^4He$ and $\delta^{18}O$ data confirm the well-known $^3He/^4He$–$\delta^{18}O$ contrast in the TMVB arc front olivines, mantle-type $^3He/^3He$ = 5.4 to 8.0 R_a combines with a high, crustal-type $\delta^{18}O$ (>5.5 to 6.6‰) (Figure 2b) (Straub *et al.*, 2015). Two new arc front olivine samples have slightly lower $^3He/^4He$ of 5.4 and 5.6 R_a, while the other 34 TMVB samples plot within the canonical depleted mantle range of 8.8 ± 2.2 Ra, which is defined by the $^3He/^4He$ range of MORB (Graham, 2002). Interestingly, the new $^3He/^4He$–$\delta^{18}O$ data for the rear-arc olivines have both have mantle-type $^3He/^3He$ = 7.7 to 8.4 R_a and mantle-type $\delta^{18}O$ (5.0 to 5.3‰).

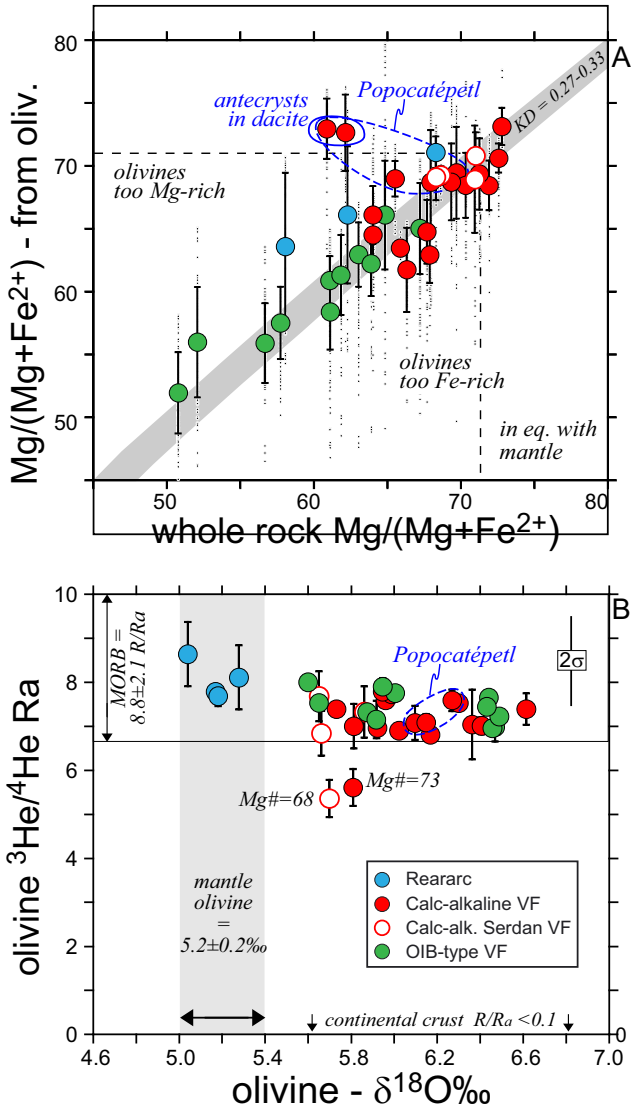

Fig. 2. TMVB olivine characteristics updated from Straub *et al.* (2015, 2011). **a.** Bulk rock Mg# [molar Mg/Mg + Fe^{2+})] vs melt Mg# from olivine per sample. Plot includes 6565 olivine analyses from 666 phenocrysts in 36 samples. Bulk rock Mg# per sample used ferric Fe calculated after Maurel & Maurel (1982) from the averaged Cr-spinel inclusions per sample (Supplementary Appendix 1). Melt Mg# from olivine is calculated with an average exchange coefficient $KD_{oliv}^{Fe/Mg}$ =0.30 ± 0.03 from Roeder & Emslie (1970), whereby $KD_{oliv}^{Fe/Mg} = [(Kd_{oliv}^{Fe}/Kd_{melt}^{Fe2+})/(Kd_{oliv}^{Mg}/Kd_{melt}^{Mg}]$. *Small dots*—individual olivine analyses per sample. *Large colored dots*—melt Mg# from olivine average per sample, with error bars denoting ±1 standard deviation. *Grey bar*—olivine/melt equilibrium for $KD_{oliv}^{Fe/Mg}$ ranging from 0.27 to 0.33. *Stippled blue circle*—Popocatépetl. *Solid blue circle*—olivine antecrysts in Popocatépetl dacites. *Stippled line*—denotes melt Mg# in equilibrium with mantle. **b.** Olivine $\delta^{18}O$‰ vs $^3He/^4He$ (R_a) of olivines for subset of n = 34 samples. $^3He/^4He$ error bars are ±1 standard deviation of individual measurement. External error is ±1 $^3He/^4He$ R_a. Two olivines with lower $^3He/^4He$ (5.4 and 5.6 Ra) are from high-MgO basalts (Cerro Pelagatos: Mg# = 73, MgO = 9.2; Serdán basalt: Mg# = 68, MgO = 8.9 wt %). MORB range of $^3He/^4He$ (R_a) of MORB after Graham (2002); $\delta^{18}O$ ‰ range of mantle olivine from Bindeman *et al.* (2022).

Olivine CaO in arc front and rear-arc magmas

Arc front and rear-arc olivines have different CaO abundances (Figure 3). The rear-arc olivines are CaO-rich (0.24 to 0.28 wt %) and overlap with MORB olivines (Díaz-Bravo *et al.*, 2014). The arc front olivines have lower CaO contents of 0.08 to 0.21 wt %. The

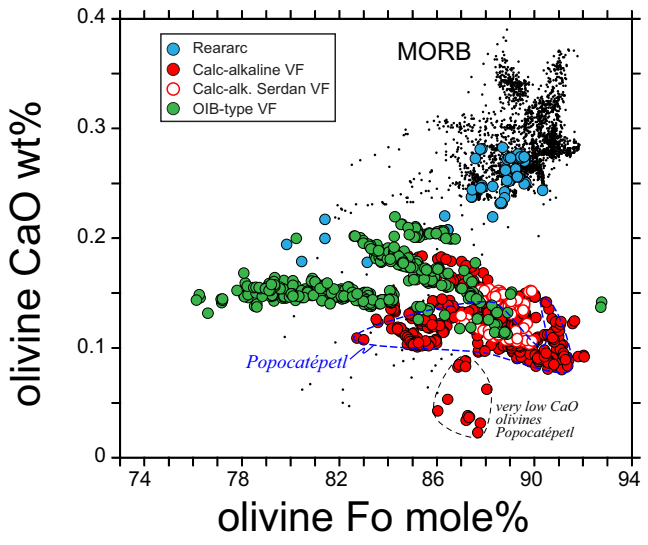

Fig. 3. TMVB olivine CaO wt % vs Fo. For clarity, only data obtained with a 900-nA beam current (n = 1272) are shown. These data mostly represent olivine cores. MORB olivines from Sobolev *et al.* (2007). *Stippled blue circle*—Popocatépetl. *Stippled black circle*—very low CaO measured in two single olivine crystals in two different samples of Popocatépetl (SPO34 and SPO38).

CaO gap between arc front and rear olivines is largest at Fo > 89, which identifies the gap as feature of the primary melts. With decreasing Fo, CaO decreases in the rear-arc olivines, but increases in the arc front olivines, which causes the trends to converge below ~Fo86 at abundances of ~0.2 wt % olivine CaO (Figure 3). Along the arc front array, olivine CaO varies by up to factor of two at a given Fo, to form a distinct, 'tiered' trend in CaO vs Fo space. There is considerable overlap between OIB-type and calc-alkaline olivines, despite the OIB-type olivines are overall shifted to higher olivine CaO and lower Fo. Calc-alkaline olivines have the lowest CaO abundances (~0.08 wt %) at the highest Fo > 89. Four single olivines from two different Popocatépetl samples (SPO38 and SPO34) have very low CaO (0.02–0.08 wt %), which is lower than the CaO of other olivines in same samples and all other calc-alkaline arc front olivines. The very low CaO olivines are shown for completeness and are not further discussed in this study.

Cr-spinel Cr# in arc front and reararc magmas

The Cr# of Cr-spinel inclusions range from 7 to 73, and display the typical, slightly inverse correlation with the Cr-spinel Mg# (Figure 4). The TMVB Cr-spinel Cr# overlaps with those of Cr-spinels in abyssal peridotites from mid-ocean ridge and forearc basalts (Dick & Bullen, 1984; Parkinson & Pearce, 1998; Pearce *et al.*, 2000; Warren, 2016; Birner *et al.*, 2017; Pearce & Reagan, 2019). Because the Cr# of mantle source and associated melts should be very similar (Clynne & Borg, 1997), the wide Cr# range suggests that the TMVB melts originate from variably depleted mantle sources. The enriched rear-arc magmas have the lower Cr# (= 19 ± 10) associated with fertile upper mantle. The OIB-type and calc-alkaline arc front magmas exhibit a much larger Cr# range at higher Cr#, which overlap with the Cr# from residual Cr-spinels from variably depleted upper mantle domains (Warren, 2016; Pearce & Reagan, 2019). The Cr# of the Cr-spinel inclusions in OIB-type and calc-alkaline olivines widely overlap, yet the Cr# in the calc-alkaline olivines is on average slightly higher than the Cr# in the OIB-type olivines.

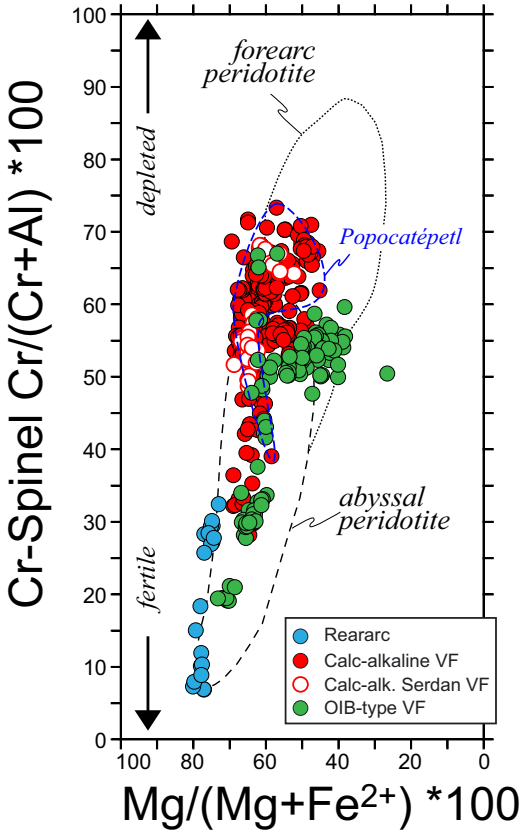

Fig. 4. Cr# vs Mg# of Cr-spinel inclusions in olivines (n = 641 data points). *Stippled blue circle*—Popocatépetl. Range of abyssal peridotite and forearc peridotite after Gamal El Dien *et al.* (2019). *Arrows* indicate fertile vs depleted upper mantle sources (e.g. Warren, 2016).

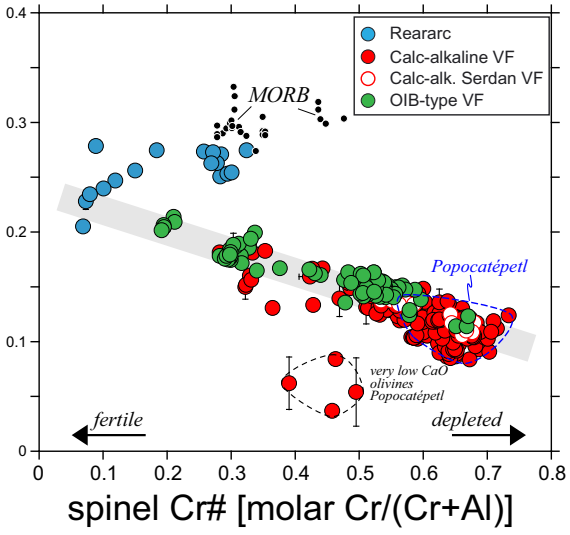

Fig. 5. Cr-spinel inclusion Cr# vs olivine CaO in TMVB olivines. Data set comprises 338 olivine–Cr–spinel pairs from 36 samples, and has a correlation coefficient of $R^2 = 0.79$, including the rear-arc olivines, but excluding the very low-CaO olivines. Error bars are ±1 standard deviation of olivine CaO and Cr-spinel Cr# average for a given olivine+Cr-spinel pair. *Stippled blue circle*—Popocatépetl. *Arrows* indicate fertile vs depleted upper mantle sources based on the Cr-spinel Cr#. MORB olivines are from Coogan *et al.* (2014)

Olivine CaO and Cr-spinel Cr# systematics

Olivine CaO + Cr-spinel Cr# pairs form a strong linear inverse correlation (Figure 5) in the OIB-type and calc-alkaline arc front series. The trend intersects with the rear-arc olivines that have the lowest Cr-spinel Cr# and olivine CaO. More CaO-rich rear-arc olivines tend to extend to lower Cr-spinel Cr# at higher CaO and aligns with MORB olivine+Cr-spinels (Coogan *et al.*, 2014). Again, OIB-type and calc-alkaline olivine+Cr-spinels widely overlap, despite a displacement of the calc-alkaline olivine+Cr-spinel pairs to higher Cr-spinel Cr# and lower olivine CaO.

DISCUSSION

The remarkable coherent, inverse correlation of arc front and rear-arc olivine CaO with the Cr# of their Cr-spinel inclusions (Figure 5) contrasts strongly with the considerable compositional diversity of their bulk rocks in major and incompatible trace elements and Sr-Nd-Pb-Hf isotope ratios (Straub *et al.*, 2011; Straub *et al.*, 2013*a*; Díaz-Bravo *et al.*, 2014; Gómez-Tuena *et al.*, 2014; Straub *et al.*, 2014; Straub *et al.*, 2015). This contrast points to a common, underlying process that controls olivine CaO and Cr-spinel Cr# and that is independent from the processes that control bulk rock composition. Because TMVB magmas ascend through a thick (~35 to ~45 km) continental basement, we first summarize the evidence against transcrustal processing - fractional crystallization and/or crustal assimilation—on the basis of the additional information provided by the extended $^3He/^4He$–$\delta^{18}O$ olivine data set.

Transcrustal processes

Source vs crustal contamination

The additional $^3He/^4He$–$\delta^{18}O$ data confirm the contrast between the high, mostly MORB-type $^3He/^4He$ and crustal-type $\delta^{18}O$ in the arc front olivines (Straub *et al.*, 2015). They do not change our previous interpretation that this signature implies melt origin from a mantle wedge that has been infiltrated by high- $\delta^{18}O$ crustal components from the slab (Straub *et al.*, 2015). The $^3He/^4He$–$\delta^{18}O$ signature cannot be reconciled with crustal basement contamination, because the uptake of ~10% to ~30% crustal materials required by the high $\delta^{18}O$, would lower melt $^3He/^4He$ to near-zero crustal R_a value (Straub *et al.*, 2015). Indeed, our previous studies found that the ^4He production rate of the old U- and Th-bearing continental crustal basement is so high, that even the tiniest (<< 1%) assimilation of basement wall rock reduces the melt $^3He/^4He$ to a near-zero R_a (Straub *et al.*, 2011; Straub *et al.*, 2013*a*; Straub *et al.*, 2014) (see also modeling in Supplementary Appendix 1).

The interpretation of an overall mantle-type $^3He/^4He$–$\delta^{18}O$ in arc front magmas is supported by the new data of the rear-arc olivines (Figure 2b), which demonstrates that a mantle-type $^3He/^4He$–$\delta^{18}O$ signature can survive the ascent through a ~ 40 km thick continental basement. All the same, the rear-arc olivines have slightly higher average $^3He/^4He$ (=8.1 ± 0.4 R_a) than the arc front olivines ($^3He/^4He = 7.2 \pm 0.6$ R_a). This offset can have several causes. First, it may reflect inherent $^3He/^4He$ variations in the upper mantle, given that all $^3He/^4He$ data are within the extended MORB range (3.5 to 15 R_a) of Graham (2002). Second, there might be traces of crustal basement contamination in the arc front magmas, as it has been proposed—but not quantified - for comparable fluctuations of olivine $^3He/^4He$ along the arc volcanic front in the Andean Northern Volcanic Zone (Lages *et al.*, 2021). However, quantification shows that the amount of crustal basement assimilated in this scenario is so tiny (<<1%) that the compositional integrity of mantle melts is not affected (Supplementary Appendix Figure S5). Thirdly, the lower arc front $^3He/^4He$

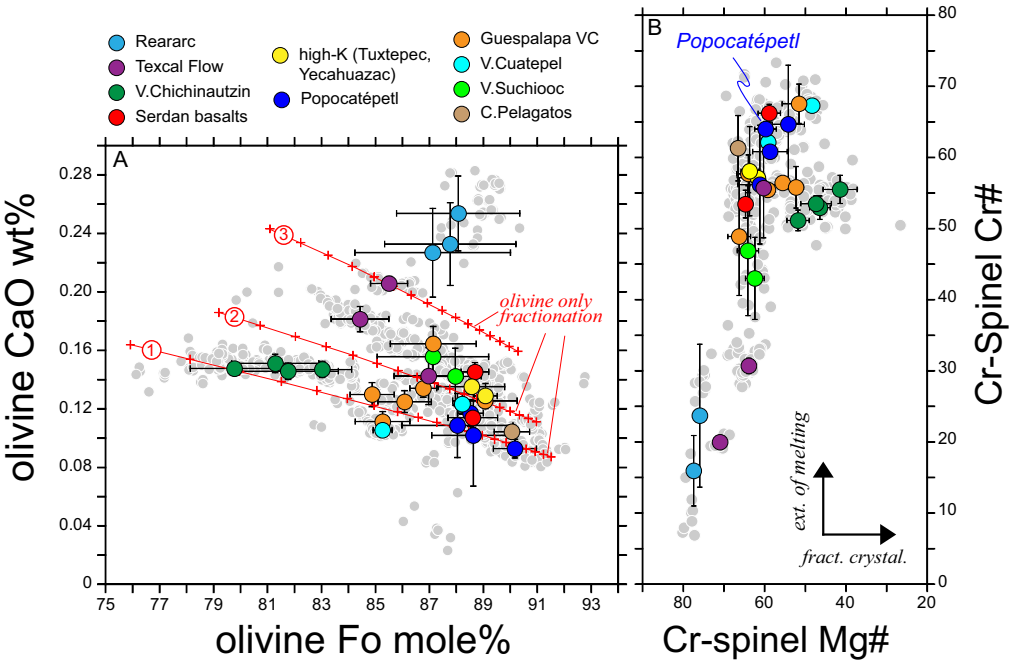

Fig. 6. a. Olivine CaO vs Fo trends. Each symbol (filled circle) represents the average olivine CaO and Cr-spinel Cr# for samples, which cannot be related by fractional crystallization (see text for criteria and data sources). Each color indicates an individual volcanic vent; same colors indicate non-cogenetic magmas from a single vent. Note end member character of Popocatépetl. Error bars are ±1 standard deviation. *Lines with red crosses*—three examples of olivine fractionation model trends in 1% steps. Starting compositions resemble observed bulk rock compositions for the TMVB and are for Trend 1: 10 MgO wt %, 5.6 wt % FeO, 4 wt % CaO, Fo = 91.5; Trend 2: 10 MgO wt %, 6 wt % FeO, 5 wt % CaO, Fo = 91; Trend 3: 10 wt % MgO, 6.5 wt % FeO, 7 wt % CaO, Fo = 90.3. Partition coefficient Kd^{Ca}_{oliv} after Jurewicz & Watson (1988). **b.** Cr-spinel Mg# [molar Mg/(Mg + Fe^{2+})] vs Cr#. Symbols as in panel a. Arrows indicate principal direction of change induced by extent of melting and fractional crystallization.

may reflect some ^{4}He ingrowth in a mantle wedge enriched by slab-derived U and Th. Any subducted ^{4}He is likely thermally lost from slab during early subduction (Straub *et al.*, 2011; Straub *et al.*, 2015), but slab recycling adds Th and U to the wedge (Straub *et al.*, 2015). However, a calculation after Ballentine & Burnard (2002) [equation 13] shows that it would take >5 to 30 million years for sufficient new radiogenic ^{4}He to ingrow in the mantle wedge in order to lower the mantle ^{3}He/^{4}He to values <5 R_a [calculation uses an initial mantle ^{4}He concentration = 4.5×10^{-11} mol/g (Sandoval-Velasquez *et al.*, 2021) and mantle ^{3}He/^{4}He = 8.5 R_a, with a mantle enriched in U ~ 0.4 μg/g and Th ~1.9 μg/g owing to slab addition]. Realistic material transfer times from slab-top to arc are much shorter, and likely well below one million years (e.g. Elliott *et al.*, 1997). In summary, while the expanded olivine ^{3}He/^{4}He–δ^{18}O data set adds more detail, it does not change our previous conclusions that the olivines crystallize in primary melts from metasomatized mantle wedge that experienced no, or negligible, crustal contamination (Straub *et al.*, 2011; Straub *et al.*, 2015).

Fractional crystallization

Another pertinent question is to which extent the major and trace elements of the olivines may have been influenced by fractional crystallization or melt mixing (e.g. Straub *et al.*, 2011; Straub *et al.*, 2013*a*; Gleeson & Gibson, 2019). At first sight, the trends of the olivine in the Fo vs CaO space mimic fractional crystallization paths (Figure 3). In the rear arc, a trend of decreasing olivine CaO with decreasing Fo points to the fractionation of an olivine +clinopyroxene +plagioclase assemblage. The trend of increasing olivine CaO with decreasing Fo at the arc front instead resembles the olivine-only fractionation trends (e.g. Blatter & Carmichael, 2001; Schaaf *et al.*, 2005) (Figure 6a).

However, the similarity to olivine-only fractionation trends at the arc front is deceptive, because most arc front magmas studied cannot be linked by fractional crystallization on the basis of their metadata (Díaz-Bravo *et al.*, 2014, Gómez-Tuena *et al.*, 2014, this study, Straub *et al.*, 2015, Straub *et al.*, 2011, Straub *et al.*, 2013*a*, Straub *et al.*, 2014). In Figure 6a, each filled colored circle denotes a sample, which is not consanguineous with any of the other samples because it has (i) distinct Sr-Nd-Pb-Hf isotope ratios; or (ii) very different incompatible trace element patterns at similar high Mg# (e.g. calc-alkaline vs high-K vs OIB-type patterns; see also Supplementary Appendix Figure S2), or (iii) olivines with distinct Ni and Fo, which cannot be connected to each other by olivine-only or olivine-dominated fractionation as discussed in our previous studies (e.g. Straub *et al.*, 2008; Straub *et al.*, 2011; Straub *et al.*, 2013*a*). In most cases, all three criteria apply, which not only separate magma batches from different volcanoes (symbols with different colors in Figure 6a), but also from the same volcanoes (same color). Previous studies also showed that the non-cogenetic relationships cannot erased by recharge melt mixing (Straub *et al.*, 2011; Straub *et al.*, 2013*a*; Díaz-Bravo *et al.*, 2014; Gómez-Tuena *et al.*, 2014; Straub *et al.*, 2014; Straub *et al.*, 2015). The primary character of the arc front magma diversity is also obvious in the wide Cr# range of the Cr-spinel inclusions (Figure 6b) which cannot be produced by fractional crystallization (Dick & Bullen, 1984; Arai, 1994; Clynne & Borg, 1997).

In summary, these observations imply that the olivine Fo-CaO variability must be primarily inherited from a range of different mantle melts that crystallize olivines with subtly variable Fo and CaO contents. This inference is consistent with the Fo-Ni systematics of the same olivines, which require melt origin from a mantle heterogeneous in Mg# (~89–92), therefore, producing a broader range primary melts in equilibrium with olivines of

~Fo87 to ~Fo91 (Straub et al., 2008; Straub et al., 2011). Of course, additional shallow fractional crystallization likely overprints the initial Fo-CaO variability in order to produce the olivine Fo-CaO range at Fo < 87 (e.g. Straub et al., 2011; Straub et al., 2013a).

Mantle processes: Extent of melting vs serial melting

What creates the strong inverse correlation of olivine CaO and Cr-spinel Cr# in the TMVB mantle melts? In the following, we first outline a potential genetic model, which is then investigated in detail.

As a simple first approximation, we assume that the olivine CaO vs Cr-spinel Cr# array is controlled by primary melt compositions. This assumption is plausible for the Cr-spinel Cr#, which is highly sensitive to melt composition and known to preserve the Cr/Al of primary mantle melts (e.g. Dick & Bullen, 1984; Kamenetsky et al., 2001). Mantle Al is stored in the aluminous phase (garnet, spinel or plagioclase) and in clinopyroxene (e.g. De Hoog et al., 2010). Al acts incompatibly during melting (e.g. Dick & Bullen, 1984), and thus melt Al decreases with the extent of melting, or with increasing mantle source depletion. In contrast, mantle Cr is primarily hosted in orthopyroxene and clinopyroxene next to spinel (Witt-Eickschen & O'Neill, 2005; De Hoog et al., 2010; Ma & Shaw, 2021). Because Cr is compatible in pyroxenes with a mineral/melt partition coefficient Kd_{px}^{Cr} »1 (e.g. Beattie et al., 1991; Ma & Shaw, 2021), melt Cr and Cr# both increase with increasing extent of melting, and they are higher in melts from depleted mantle (e.g. Dick & Bullen, 1984; Kamenetsky et al., 2001).

CaO is incompatible in olivine and strongly sensitive to melt CaO (e.g. Jurewicz & Watson, 1988). Melt CaO in primary melts is controlled by mantle clinopyroxene, which is the exclusive host of mantle CaO (Langmuir et al., 1992; De Hoog et al., 2010). A fertile mantle with ~13–18 wt % clinopyroxene produces CaO-rich melts, whereby melt CaO increases with the extent of melting as long as clinopyroxene is residual in source until ~22–29% melt extraction (=clinopyroxene-out) (e.g. Langmuir et al., 1992; Bizimis et al., 2000). However, because clinopyroxene melts out faster than olivine and orthopyroxene, the proportion of clinopyroxene in the residual mantle decreases more rapidly than mantle olivine and orthopyroxene during melting (Langmuir et al., 1992; Bizimis et al., 2000). Thus, as mantle clinopyroxene decreases in source, melt CaO should also decrease with progressive source depletion at a given extent of melting.

Together, this systematics may explain the olivine CaO vs Cr-spinel Cr# array as product of repeated or 'serial' melt extraction from a given parcel of mantle in the presence of residual clinopyroxene. 'Serial melting' is the repetitive melting of the same source, which may proceed until the source becomes too refractory to melt at the clinopyroxene-out, beyond which melting requires much higher mantle temperatures (Hess, 1994; Kushiro, 2001) or additional water (Parman & Grove, 2004). In the arc environment, serial melting is plausible, because the slab flux to the mantle wedge is continuous as seen from studies of supra-subduction zone peridotites (e.g. Bizimis et al., 2000), and thus should trigger serial melt events within the lifetime of individual arc volcanoes (Straub & Martin-Del Pozzo, 2001; Streck et al., 2002; Straub et al., 2013a; Larrea et al., 2019). Because the frequency of melting outstrips mantle replenishment by the slower convective corner flow (~10–100 km per million year, Ficini et al., 2017), serial melting should be efficient in depleting the background mantle (=mantle without slab component) 'in-situ' beneath active arc volcanoes.

In the TMVB, mantle depletion by serial melting has been previously proposed based on the bulk rock incompatible elements and olivine Fo-Ni systematics (Straub et al., 2008; Straub et al., 2013a; Straub et al., 2014; Straub et al., 2015). Here we propose that is also a suitable mechanism to explain the olivine CaO vs Cr-spinel Cr# systematics. Importantly, the inverse array cannot be created by simply increasing the extent of melting, as proposed by Dick & Bullen (1984) for a similar Cr-spinel Cr# range in MORB. This is because an increasing extent of melting predicts a positive correlation in the olivine CaO vs Cr-spinel Cr# space. In addition, a variable extent of melting of the same source is at variance with the missing consanguinity of the melts evident from the olivine+Cr-spinels which construct the array (Figure 6b).

While the 'serial melting model' (as it will be referred to hereafter) may account for the coherent olivine CaO vs Cr-spinel Cr# systematics, it builds on several assumptions, which are: (i) olivine CaO primarily reflects melt CaO; (ii) primary melt CaO, Al or Cr concentrations are not affected by secondary pyroxenites in source; and (iii) the slab-flux drives the serial melting and mantle source depletion at the arc front. These assumptions will be discussed next.

Controls on olivine/melt CaO partitioning

Experimental CaO partitioning between olivine and melt

CaO is incompatible in olivine with Kd_{oliv}^{Ca}'s mostly below 0.1 (Jurewicz & Watson, 1988; Beattie et al., 1991; Libourel, 1999; Laubier et al., 2014; Ma & Shaw, 2021). Experimental studies confirm strong links between melt and olivine CaO, whereby the Kd_{oliv}^{Ca} was found to be indifferent to the pressure of crystallization below 2 GPa, melt temperature, melt oxygen fugacity (Jurewicz & Watson, 1988; Beattie et al., 1991; Libourel, 1999; Laubier et al., 2014), and melt polymerization (Wang & Gaetani, 2008). However, some compositional dependencies exist. First, the Kd_{oliv}^{Ca} increases slightly with decreasing olivine Fo, because Ca^{2+} substitutes more easily for the slightly larger Fe^{2+} cation site than for the Mg^{2+} site (e.g. Jurewicz & Watson, 1988; Libourel, 1999; Ma & Shaw, 2021). Second, the Kd_{oliv}^{Ca} can decrease with increasing melt H_2O (Feig et al., 2006), which may lower the olivine CaO in hydrous, undegassed arc magmas (Gavrilenko et al., 2016).

Quantifying the olivine-melt partitioning for CaO in the TMVB is not simple, because there are no internally consistent partitioning data. Different approaches and various parametrizations in the partitioning studies have returned a large (up to a factor of 10) range of Kd_{oliv}^{Ca} at a given Fo (Supplementary Appendix Figure S6). However, the high Kd_{oliv}^{Ca}'s (~0.12 to 0.22) predicted by Libourel (1999) do not apply in the TMVB, because they are optimized for Fe- and alkali-rich melts with far lower olivine Fo < 80 than the TMVB olivines. The intermediate Kd_{oliv}^{Ca}'s (~0.04 to 0.12) of Beattie et al. (1991) seem uncertain, because they build on an only weak dependency of the Kd_{oliv}^{Ca} on the Kd_{oliv}^{Mg}.

The lowest Kd_{oliv}^{Ca}'s (~0.01 to 0.04) are obtained by the parametrization from Jurewicz & Watson (1988), which includes a correction for the olivine FeO (Figure 7a). The Jurewicz & Watson (1988) Kd_{oliv}^{Ca}'s coincide with those of Laubier et al. (2014) and Ma & Shaw (2021). These Kd_{oliv}^{Ca}'s apply for anhydrous high-Mg# basalts and basanites from mid-ocean ridges, and arc and intraplate settings. They seem most realistic for the TMVB, also because they overlap with a Kd_{oliv}^{Ca} calculated with the TMVB samples (Figure 7b). This calculated Kd_{oliv}^{Ca} is obtained by dividing the average CaO of all equilibrium olivines in a given sample by the bulk rock CaO. Equilibrium olivines are those that have an olivine/bulk rock Fe^{2+}/Mg exchange coefficients ($KD_{oliv}^{Fe/Mg}$) between 0.27 and 0.33. The calculation uses a bulk rock ferric Fe_2O_3 that

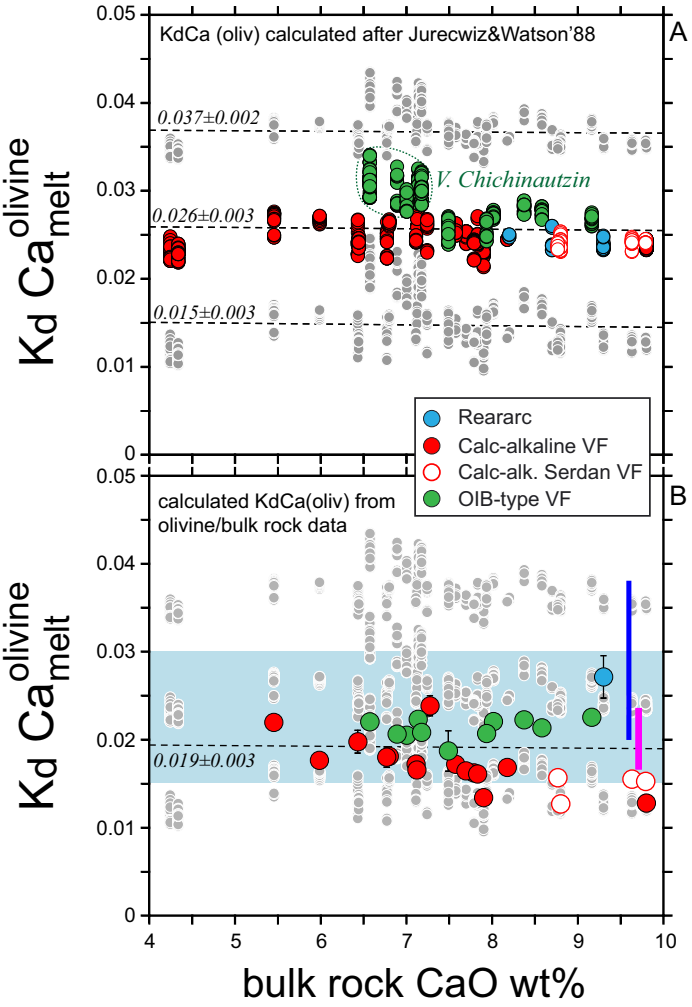

Fig. 7. Kd^{Ca}_{oliv} vs bulk CaO wt % for 900 nA olivine data. **a.** Kd^{Ca}_{oliv} calculated from the olivine Fo after Jurewicz & Watson (1988) [Kd^{Ca}_{oliv} = 0.01∗(−0.08 ± 0.015) ∗Fo + (9.5 ± 0.2)]. *Colored symbols*—average Kd^{Ca}_{oliv} = 0.026 ± 0.003 after from Jurewicz & Watson (1988); *grey symbols with stippled lines*—minimum (0.015 ± 0.003) and maximum (0.037 ± 0.002) Kd^{Ca}_{oliv} after Jurewicz & Watson (1988). Note slightly elevated Kd^{Ca}_{oliv} from Fe-rich V. Chichinautzin olivines that may not be fully corrected by the Jurewicz & Watson (1988) parametrization. **b.** Kd^{Ca}_{oliv} calculated from bulk rock and olivine averages (n = 31 samples), using only olivines in Fe/Mg equilibrium with bulk rock (see text for filtering). Error bars (± stdev) of averaged olivine are mostly within symbol size. Results are compared to Kd^{Ca}_{oliv} after Jurewicz & Watson (1988) (*grey dots*, as in panel a), Laubier *et al.* (2014) (*dark blue bar*) and Ma & Shaw (2021) (*pink bar*). *Light blue field*—the range of Kd^{Ca}_{oliv} (~0.015 to 0.030) induced by variable melt water content from ~2 to 6 wt % H_2O (Gavrilenko *et al.*, 2016).

was obtained after Maurel & Maurel (1982) from the average stoichiometric Fe^{3+}/Fe^{2+} of all Cr-spinel inclusions per sample (Supplementary Appendix 1, Supplementary Appendix Figures S5 and S6). The percentage of melt Fe_2O_3 ranges between 9–20%, with an average of 12 ± 3%, which is plausible for primitive arc magmas (e.g. Kelley & Cottrell, 2009). Approximately half (~51%) of the olivines from 31 samples (out of 36 samples) are in equilibrium with their respective bulk rocks. These olivines return a calculated Kd^{Ca}_{oliv} of 0.019 ± 0.003 (Figure 7b) with a total range by a factor of ~2 (0.013 to 0.027). This range is considered acceptable since the calculated Kd^{Ca}_{oliv} depends on how well the average olivine CaO approximates the 'true' average olivine CaO in the TMVB magmas where crystal-scale mixing is common (e.g.Straub *et al.*, 2008 ; Straub *et al.*, 2011).

The calculated Kd^{Ca}_{oliv}'s are within the uncertainty range of the Kd^{Ca}_{oliv}'s of Jurewicz & Watson (1988) (0.012 to 0.046; grey dots in Figure 7b). The Jurewicz & Watson (1988) equation provides slightly higher Kd^{Ca}_{oliv}'s for the Fe-rich magmas from V. Chichinautzin, but this effect is within the uncertainty range. Thus, no perceptible change in Kd^{Ca}_{oliv} is expected at the high Fo (~80–90) of the TMVB olivines. Moreover, the validity of the calculated Kd^{Ca}_{oliv} is supported by its independence from bulk rock CaO (~5.5 to 10 wt %) (Figure 7).

How sensitive is the Kd^{Ca}_{oliv} to melt H_2O?

The light blue field in Figure 7b displays the Kd^{Ca}_{oliv} range (~0.015 to 0.030) that corresponds to an increase in melt water content from ~2 to ~6 wt % H_2O (Gavrilenko *et al.*, 2016). This is similar to the known range of melt water (~0.2 to 5.2 wt % H_2O) in the TMVB magmas (Cervantes & Wallace, 2003*a*; Cervantes & Wallace, 2003*b*; Johnson *et al.*, 2009; Roberge *et al.*, 2009), and thus implies that the influence of water on the Kd^{Ca}_{oliv} is within the overall uncertainty range. Consequently, it is not possible - with the partitioning data at hand - to quantify or even to discern an effect of melt water on the Kd^{Ca}_{oliv} in the TMVB.

Nevertheless, some inferences on the proposed influence of melt water on olivine CaO can be made from the TMVB olivines

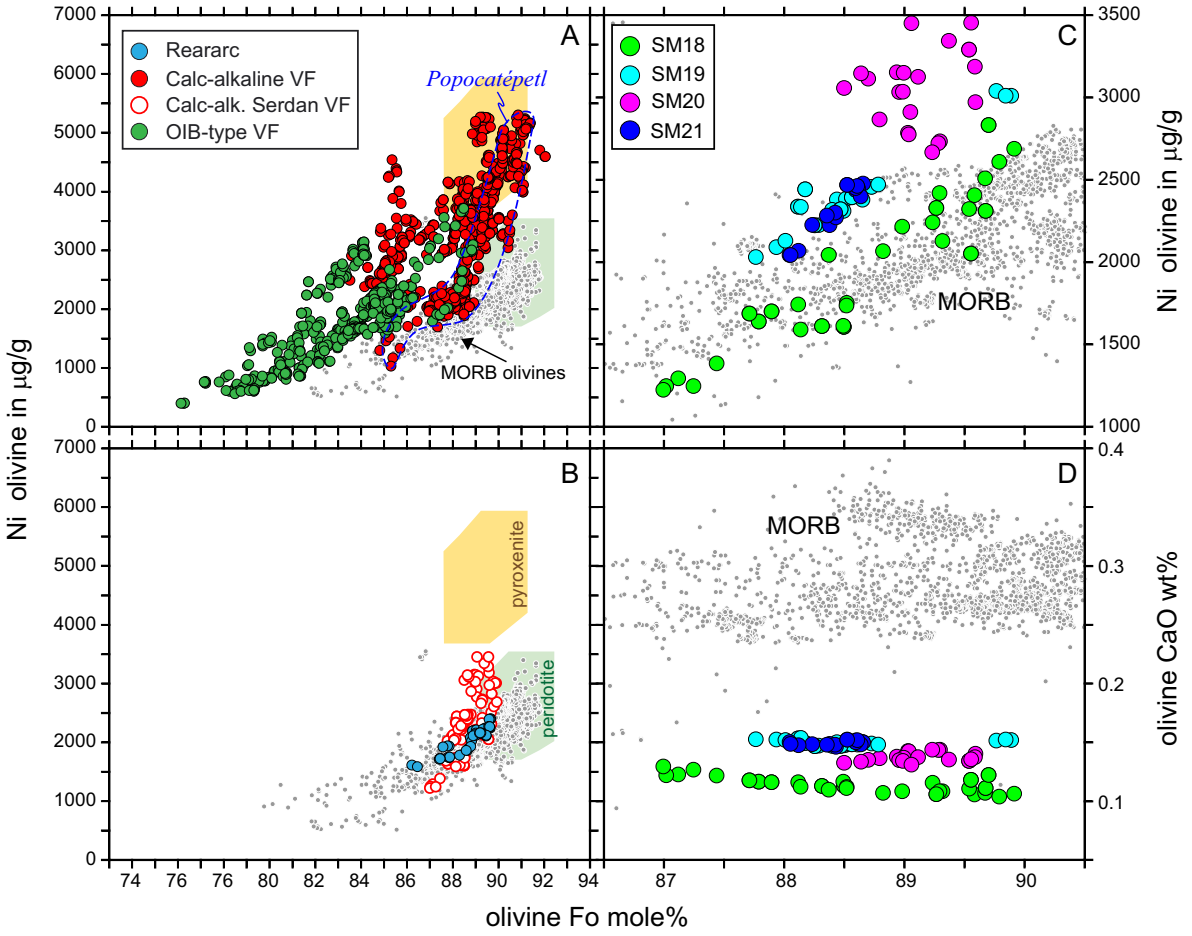

Fig. 8. a, b: Olivine Ni (μg/g) vs Fo overview of TMVB olivines studied. *Small grey dots*—MORB olivines after Sobolev *et al.* (2007). *Stippled blue circle*—Popocatépetl. Fields of olivines in equilibrium mantle peridotite (*green*) and reaction pyroxenite (*brown*) from Straub *et al.* (2011, 2008). **c:** Olivine Ni (μg/g) vs Fo of Serdán basalts **d:** Olivine CaO (wt %) vs Fo for Serdán basalts. For discussion see text.

themselves. A solid result of olivine melt inclusion studies was that the calc-alkaline magmas are more hydrous (up 5.2 wt % melt H_2O) (Moore & Carmichael, 1998; Cervantes & Wallace, 2003*a*; Roberge *et al.*, 2009) than the OIB-type magmas, which are only moderately wet with ~0.2–1.3 wt % H_2O (Cervantes & Wallace, 2003*b*; Johnson *et al.*, 2009). TMVB rear-arc magmas are dry to moderately wet ($H_2O \sim 0$–2.3 wt %) based on plagioclase hygrometry (Díaz-Bravo *et al.*, 2014). However, there are no offsets between calc-alkaline and OIB-type olivines in the CaO vs Cr-spinel Cr# space, which must be present if the Kd^{Ca}_{oliv} was strongly influenced by the melt water content. Instead, the data for all arc front series overlap. Possibly this means, that all olivines studied crystallized late in already degassed melts, in which case the olivine CaO would reflect the melt CaO anyway. In summary, while uncertainties due to the partitioning data exist, the existing data argue against a strong influence of either FeO or H_2O on olivine CaO, even if minor effects are possible. Instead they agree with melt CaO being the dominant control of the TMVB olivine CaO.

The decoupling of olivine Ni and CaO in arc front magmas

Most of the TMVB olivines investigated are 'high-Ni olivines' (Figure 8) have been linked to the presence of secondary mantle pyroxenites. Sobolev *et al.* (2005) first proposed for the intraplate environment, that secondary pyroxenites may form following the reactive infiltration of silica-rich materials in the mantle source. This would cause mantle olivine to be replaced by new secondary orthopyroxenes and clinopyroxenes. Subsequently, it was proposed that the secondary clinopyroxene increases the total amount of clinopyroxene in source, which would increase CaO retention in source, and reduce CaO in partial melts and their magmatic olivines (e.g. Herzberg, 2006; Søager *et al.*, 2015; Zamboni *et al.*, 2017).

One problem with this hypothesis is that decompression melting models predict an increase (not a decrease) in melt CaO with the increasing amount of clinopyroxene in source, because clinopyroxene is the main phase melted (e.g. Langmuir *et al.*, 1992). Another problem is that it predicts that low CaO arc olivines must be coupled with high-Ni contents. The latter is not observed in the TMVB, where low CaO arc front olivines have variable Ni. High-Ni olivines are common in the Sierra Chichinautzin/Popocatépetl area (Straub *et al.*, 2008; Straub *et al.*, 2011), but lack in the Serdán basalts, where olivine have both low Ni and CaO (Figure 8b). Within the Serdán basalts, olivine CaO and Ni do not co-vary either: the olivines with the highest Ni (SM20) do not have the lowest CaO, which is instead found in the olivines with the lowest Ni contents (SM18). Thus, it seems that olivine Ni and CaO can be decoupled in arc front magmas, which argues against a joint control by secondary mantle pyroxenites.

The decoupling of olivine Ni and CaO is simple to explain, if one considers two independent controls: while the olivine Ni depends on the presence or absence of mantle olivine, olivine CaO

should be dependent on the amount of mantle clinopyroxene at a given extent of melting (Langmuir *et al.*, 1992). Notably, in the 'arc variant' of the Sobolev *et al.* (2005) model, no additional secondary clinopyroxene is required beyond the replacement of mantle olivine by orthopyroxene (Straub *et al.*, 2008; Straub *et al.*, 2011). Thus, serial melting should lower melt CaO as mantle clinopyroxene progressively decreases, regardless of peridotite or pyroxenite source. However, if mantle olivine was not, or only partially eliminated in the mantle wedge, the melt Ni does not increase and magmatic olivines had low Ni contents. High-Ni contents in low CaO olivines would only occur, if the olivine-to-orthopyroxene transformation was complete. This decoupling may well explain why low CaO arc olivines are far more common than high-Ni arc olivines—simply, because the complete elimination of mantle olivine by the reactive silicic slab flux is more difficult to achieve than a reduction of clinopyroxene by serial melting.

The driver of serial melting beneath the arc volcanic front

The obvious driver for serial melting is the hydrous silicic slab flux, which triggers melting by lowering the solidus, and creates the secondary, more fusible pyroxenite lithologies (Straub *et al.*, 2008, Straub *et al.*, 2011). Extensive studies of arc—forearc/trench compositional links in the TMVB leave little doubt that the slab flux strongly influences the composition of the TMVB arc front magmas (e.g. Gómez-Tuena *et al.*, 2007; Straub *et al.*, 2015; Parolari *et al.*, 2018; Gómez-Tuena *et al.*, 2018*a*; Gómez-Tuena *et al.*, 2018*b*; Parolari *et al.*, 2021).

The connection between the slab flux (triggers serial melting) and mantle depletion (by serial melting) can be tested by correlating the crystal tracers of mantle depletion (e.g. Cr-spinel Cr#, olivine CaO) with bulk rock incompatible element ratios that are 'mantle-controlled' (not added from slab), or 'slab-controlled' (dominated by the slab flux), respectively. In the TMVB high-Mg# magmas, where Ti-Fe-oxides are absent, only a few incompatible elements are mantle-controlled, which include TiO_2 and the heavy REE Ho, Er, Yb and Lu (Straub *et al.*, 2014). The bulk rock TiO_2/Lu with the largest contrast in elemental incompatibility is most sensitive to mantle source variations. Interestingly, the total range of TiO_2/Lu in the TMVB volcanic rock cannot be reproduced by a single melting step, but requires at least one re-melting of the source (Straub *et al.*, 2014). As predicted by the serial melting model, the average Cr-spinel Cr# per sample increases with decreasing bulk rock TiO_2/Lu (Figure 9). The array is bracketed by rear-arc basalts (enriched) and Popocatépetl Cr-spinels (depleted), respectively. The TMVB TiO_2/Lu range of ~2.5 to 6 is also within with the only slightly larger TiO_2/Lu range in MORB (~2 to 6) (Gale *et al.*, 2013), as expected if TiO_2/Lu traces melting of the upper mantle.

Conversely, Cr-spinel Cr# correlates positively with tracers of slab flux, such Ba/La, Nd/Pb, Nb/La, Li/Ho and especially $^{87}Sr/^{86}Sr$ (Figure 9b). Importantly, the covariation of Cr# with $^{87}Sr/^{86}Sr$ confirms that the slab flux imposes heterogeneity on the mantle wedge, as the low $^{87}Sr/^{86}Sr$ of the original mantle (~rear-arc mantle) becomes increasing augmented by the radiogenic slab flux that is at its peak where the background mantle is most depleted (higher Cr#).

Insights from the trends of arc-front monogenetic volcanoes

The olivines of monogenetic volcanoes cover the entire array of arc front olivines in the CaO vs Cr-spinel Cr# space (Figure 10). Because the spatial, temporal and compositional relationships of monogenetic eruptive lava flows and pyroclastic deposits are far easier to unravel than those of the complex composite volcanoes, their variations provide additional constraints for the serial melting model proposed. Key insights are:

The evolution of the residual mantle

Time series from monogenetic volcanoes illustrate how efficiently serial melt extraction can modify the residual mantle. The best example is provided by the OIB-type Texcal Flow that is constructed by at least three individual lava flows, which in the order of eruption, are the 'Old Texcal Flow', the 'Main Texcal Flows' and the 'Cuescomates vents lavas' (Figure 10a) (Straub *et al.*, 2013*a*). Each unit has distinct incompatible element and isotope ratios (Straub *et al.*, 2013*a*) which systematically change with their average olivine+Cr-spinels (~0.21 wt % CaO / Cr# ~ 20; ~0.18 wt % ~31 and ~ 0.14 wt %/~55; Figure 10a). For example, with increasing Cr-spinel Cr#, bulk rock Nd/Pb decreases from ~8 to ~6, Nb/La from 1.2 to 0.9 and TiO_2/Lu from 4.6 to 4.0, while $^{87}Sr/^{86}Sr$ increases from 0.7031 to 0.7038 and La/Lu from 38 to 62 (Straub *et al.*, 2013*a*). Remarkably, together the three Texcal flows define a straight trend across most of CaO vs Cr-spinel Cr# space (Figure 10a). This suggests that serial melt extraction may induce profound changes in the local mantle source of a monogenetic volcano within its short lifetime, typically on the scale of years.

While similar time series are not available for the monogenetic volcanoes, their variations confirm that serial melting may induce considerable local source heterogeneity. For example, the Guespalapa Volcanic Complex (Figure 10b) consists of a volcanic shield which is topped by three small cones (El Caballito, Manteca and El Hoyo) that are spaced only a few 100 meters apart (Siebe *et al.*, 2004*b*). The shield and each cone have distinct bulk rock Sr-Nd isotope ratios and/or trace elements (Straub *et al.*, 2014) as well as distinct olivine CaO, Ni and Cr-spinel Cr# signatures, and are, therefore, not consanguineous. The range of olivine CaO-Cr-spinel Cr# at Guespalapa is nearly as large as at the Texcal Flow, with a displacement to higher Cr#. This suggests that Guespalapa melts were sourced from a mantle locally made heterogeneous by serial melting. Similar systematics occur also at less complex monogenetic volcanoes, such as at calc-alkaline volcano Cuatepel, where olivine+Cr-spinels of cones and flow also correlate inversely (Figure 10c), or also at regional scale seen from the Serdán group, where the basalt flow (SM18) closest to the arc front is offset to lower olivine CaO at higher Cr# relative to the three basalts ~15 km farther to the north (higher CaO) (Figure 10d).

A notable exception from the broader variability of olivine+Cr-spinels is the OIB-type monogenetic V. Chichinautzin. Each of its four consecutive eruptive units has distinct major and trace elements and Sr-Nd isotope ratios (Siebe *et al.*, 2004*a*; Straub *et al.*, 2013*a*), and yet the range in Cr-spinel Cr# is small and varies only from 51 to 56 (Figure 10e). Olivine CaO is indistinguishable in the four units. Still, the oldest V. Chichinautzin flows have a lower average Cr-spinel Cr# ($=51 \pm 1$) than the youngest lavas ($Cr\# = 56 \pm 2$), and both bracket the intermediate lavas ($Cr\# = 53 + 2$ and $Cr\# = 54 \pm 1$, respectively). With ~1 km^3 eruptive volume, V. Chichinautzin is the largest of all Sierra Chichinautzin monogenetic volcanoes (Siebe *et al.*, 2004*b*). Here, it seems possible that despite the isotopic and trace element diversity of the V. Chichinautzin series, the residual mantle was locally barely affected by melt extraction.

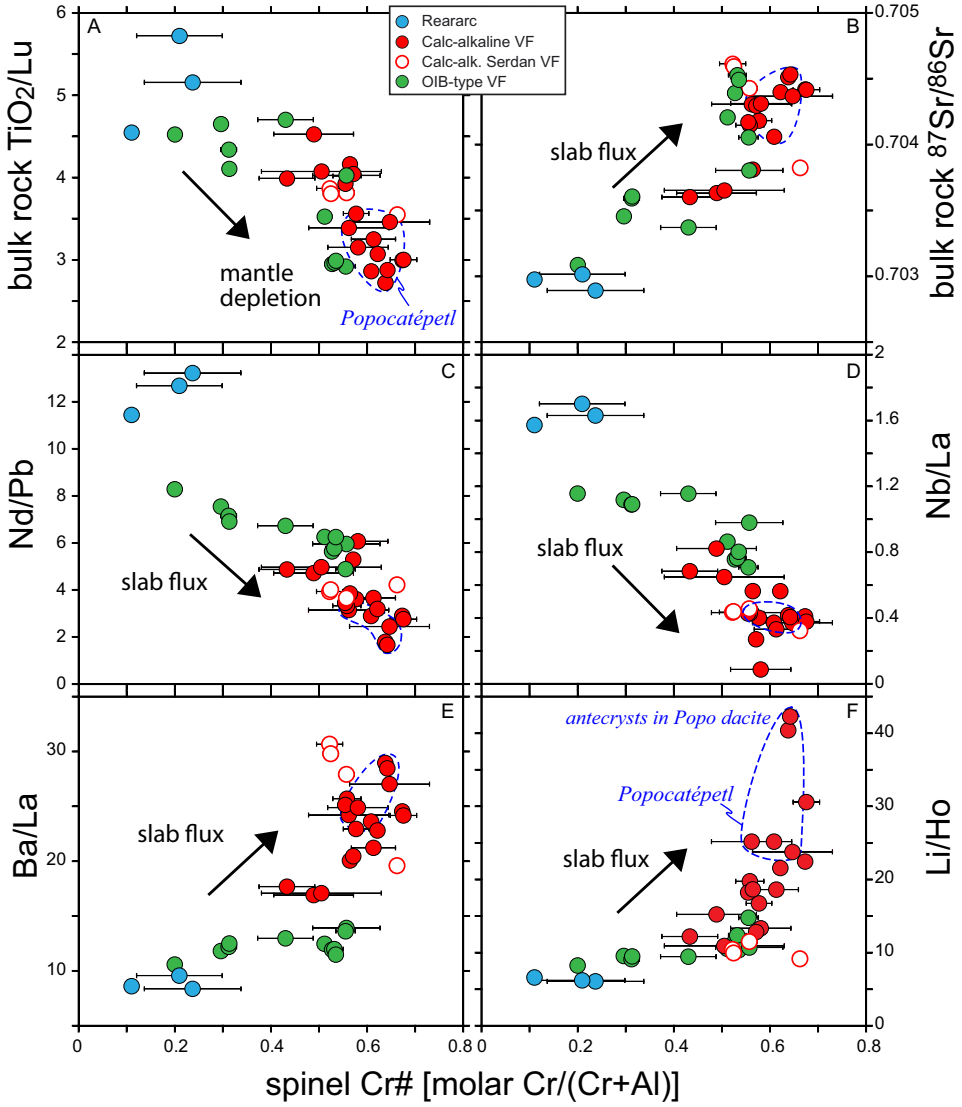

Fig. 9. Average Cr# of Cr-spinel inclusions vs bulk rock composition. Error bars are 1 standard deviation of the average Cr# from all Cr-spinels per sample. (**a**) Cr# vs bulk rock TiO_2/Lu (proxy for mantle source depletion), (b–f) Cr# vs proxies for slab flux bulk rock ($^{87}Sr/^{86}Sr$, Nd/Pb, Nb/La, Ba/La and Li/Ho. Bulk rock data from Gómez-Tuena et al. (Gómez-Tuena *et al.*, 2014), Díaz-Bravo *et al.* (2014) and Straub *et al.* (2015). *Stippled blue circle*—Popocatépetl range. For discussion see text.

Coexistence of OIB-type vs calc-alkaline arc front magmas

Another remarkable observation of the monogenetic trends is the wide overlap between OIB-type and calc-alkaline olivine+Cr-spinels (Figs. 5, 10). Antecryst uptake does not explain this overlap because calc-alkaline and OIB-type vents are spatially and temporally separated, and thus do not share a plumbing system where the crystal cargo can be exchanged. This is also true for the Suchiooc Cone (calc-alkaline) and the immediately adjacent Suchiooc Flows (OIB-type): olivine+Cr-spinels overlap (Figure 10f) despite distinct bulk rock major and trace element and Sr-Nd isotope composition (Straub *et al.*, 2014), yet there is no shared plumbing system as the flow visibly postdates the cone based on field observations.

The olivine+Cr-spinels provide no support for the hypothesis that calc-alkaline magmas may originate from a residual mantle after OIB-type melt extraction (e.g. Wallace & Carmichael, 1999; Cervantes & Wallace, 2003*a*; Straub *et al.*, 2008; Johnson *et al.*, 2009). This would predict systematically lower olivine CaO and higher Cr-spinel Cr# in the calc-alkaline magmas than the OIB-type magmas. Moreover, it disagrees with the chronology of the volcanic events in the Sierra Chichinautzin Volcanic Field, where the young (<2000 years) OIB-type series follow the Holocene calc-alkaline magmas (Siebe *et al.*, 2004*b*; Straub *et al.*, 2013*b*). The simplest explanation for the overlapping olivine+Cr-spinel compositions is that the source domains of the calc-alkaline, high-K and OIB-type magmas co-exist in the mantle wedge, and each is modified according to its own individual melt extraction history.

No liquid-line-of-descent from basalt to andesite

The olivine+Cr-spinel systematics should capture earliest stages of melt evolution after the liquidus. We note that the signals recorded by the olivine+Cr-spinels do not conform to experimental liquid-line-of-descents, that produce andesitic melts from basaltic parental melts. Blatter *et al.* (2013) and Muentener & Ulmer (2018) obtained successful liquid-line-of-descents for the basalt to andesite evolution in dry and hydrous experiments at arc-typical elevated oxygen fugacities and at pressures corresponding to middle to deep arc crust (up to 45

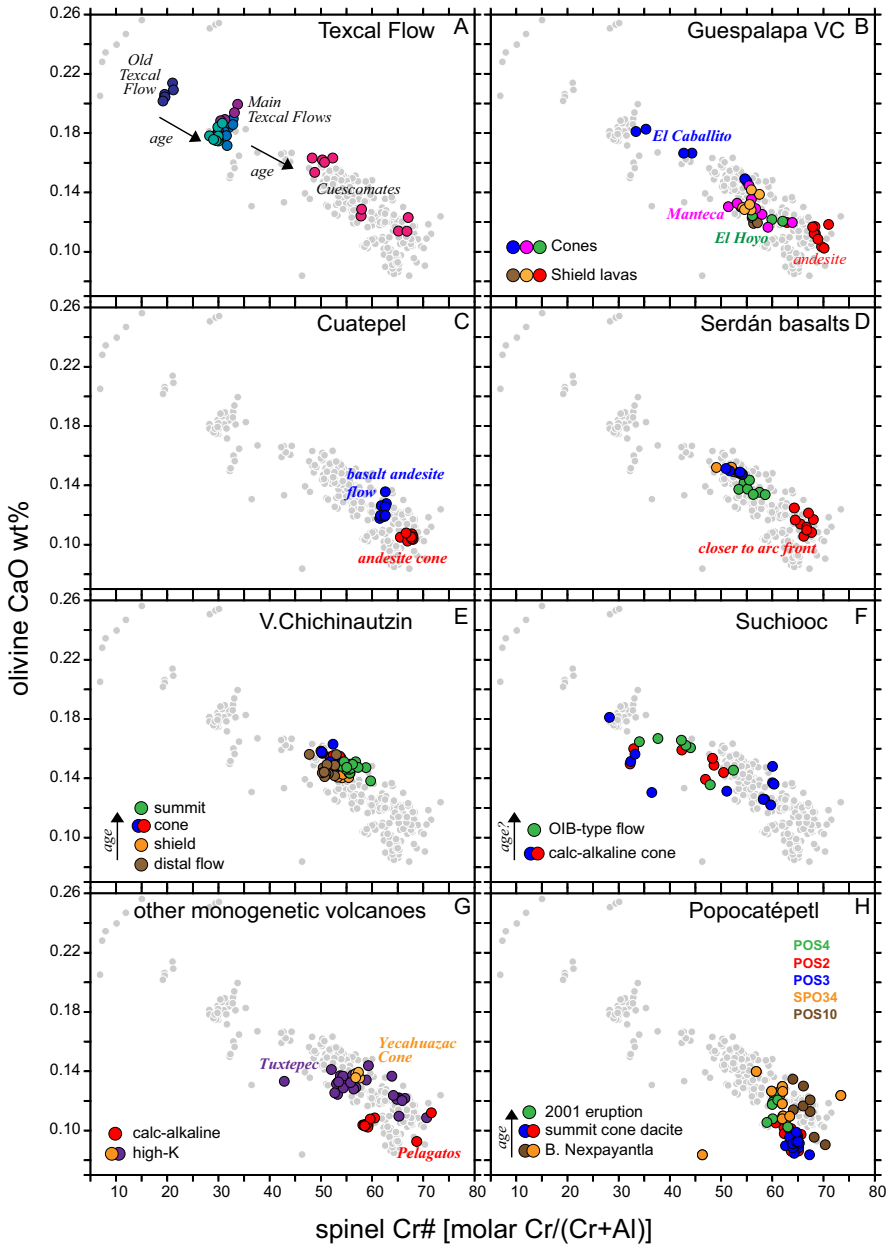

Fig. 10. Olivine CaO vs Cr-spinel Cr# for several monogenetic and one composite volcanos. a. Texcal Flow (OIB-type) b. Guespalapa Volcanic complex (calc-alkaline) c. Cuatepel (calc-alkaline) d. Serdan basalts (calc-alkaline) e. V. Chichinautzin (OIB-type) f. Suchiooc (OIB-type and calc-alkaline) g. Other monogenetic cones (Pelagatos, Yecahuazac, Tuxpetec) (calc-alkaline/high-K) h. Popocatépetl. See text for discussion

kilometers). In the experiments, melt CaO always decreases with increasing SiO_2, while melt Al_2O_3 increases the earliest stages of differentiation. The interval of increasing Al_2O_3, which is largest in hydrous melt, is caused by early pyroxene crystallization in the absence of plagioclase (Blatter *et al.*, 2013; Muentener & Ulmer, 2018). While one could argue that melts in the middle to deep crust follow their own fractionation path, this sequence is not mimicked by the forsteritic olivine+Cr-spinels. Melt Cr has not been measured in these experiments, but it is reasonable to assume that melt Cr decreases as it is consumed by pyroxenes and Cr-spinel. Thus, melt Cr# will decrease with decreasing CaO, which is opposite to the trend of the olivine+Cr-spinels (Figures 5,10). Additionally, the experiments predict that Cr# decreases with increasing melt SiO_2, which is also opposite to the observed trend of increasing Cr-spinel Cr# with increasing melt silica (Figure 11).

This latter increase is also visible in the monogenetic volcanoes. For example, at the Cuatepel volcano, the andesite (Cr# = 67 ± 1) has higher Cr# than the basaltic andesite flow (Cr = 62 ± 1). At the Texcal Flow, an increase in melt silica from 50.0 to 52.6 wt % SiO_2 correlates with a large increase in Cr-spinel Cr# from 20 ± 1 to 56 ± 7. Moreover, the high-MgO monogenetic basalts or basaltic andesites, which should best approximate mafic parental melts, do not always have the highest Cr-spinel Cr#. For example, the Tuxtepec basalt (MgO = 9.8 wt %; Mg# =72) has Cr-spinel with Cr# =61 + 4, and the Pelagatos basaltic andesite (MgO = 9.1 wt %; Mg# =73) has Cr-spinels with Cr# =58 ± 6 (Figure 10g). Instead, the Cr-spinels with the highest Cr# occur always in the andesites of the monogenetic fields (e.g. Guespalapa shield andesite Cr# =68 ± 3) and of Popocatépetl (e.g. Nexpayantla andesite Cr# = 65 ± 3) (Figs. 10h, 11). While the olivine+Cr-spinels argue against melt

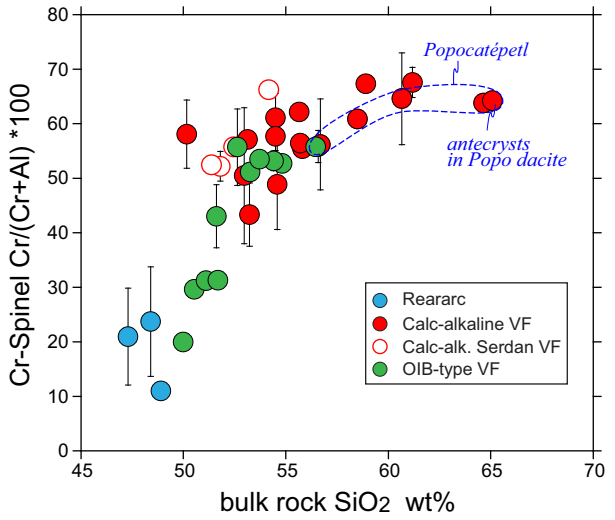

Fig. 11. Bulk rock SiO_2 wt % vs average Cr-spinel Cr# per sample. *Stippled blue circle*—Popocatépetl, including olivine+Cr-spinel antecrysts in Popocatépetl dacites. Error bar are ±1 standard deviation of average Cr# per sample. See text for discussion

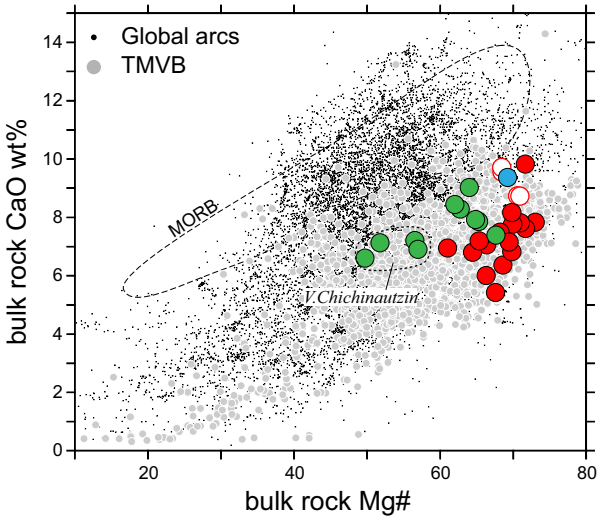

Fig. 12. Bulk rock Mg# vs CaO in global arcs. Arc data are from GeoROC (2023), Straub (2019); MORB data are from Gale *et al.* (2013). Highlighted TMVB samples (n = 31) are only those where equilibrium olivines were found in bulk rock (see Figure 7b); samples with olivine+Cr-spinel antecrysts are not shown. V. Chichinautzin stands out by its inherently high FeO/MgO.

evolution by fractional crystallization, they readily conform with genetic models that propose that a broader spectrum of basaltic to andesitic primary mantle melts originates from variably depleted mantle sources in the TMVB (Straub *et al.*, 2008; Straub *et al.*, 2011).

The origin of mantle depletion beneath composite volcano Popocatépetl

Lastly, the monogenetic olivine+Cr-spinel trends have implications for magma genesis at composite volcano Popocatépetl. Popocatépetl has end member character in olivine CaO + Cr-spinel Cr# space (Figure 10h). In the context of the serial melting model, this suggests that Popocatépetl mafic melts are extracted from a highly depleted background mantle. At first sight, taken by itself and given the much larger eruptive volume of Popocatépetl (~500 km^3), one might attribute the source depletion at Popocatépetl to a larger extent of melting that is driven by a high, hydrous slab flux to its source. However, the position of Popocatépetl at the high-Cr# end of the olivine+Cr-spinel array, that is principally constructed by the small volume (≤1 km^3) monogenetic volcanoes imply that the Popocatépetl source domain may have also evolved by serial melting from an original rear-arc-type mantle. In other words, the source depletion at Popocatépetl should have also developed by serial extraction of small-volume mantle melts comparable to those that build the monogenetic volcanoes. These melts must have been extracted frequently and for a long time to sustain a steady influx of mafic melts into the Popocatépetl plumbing system.

Popocatépetl has been active since at least several 100 000 years (e.g. Cadoux *et al.*, 2011). The samples studied range from the oldest exposed basaltic andesite and andesite flows of the Barranco Nexpayantla (erupted several 100 000 years ago) to the andesites and dacites from the active summit cone, some of which are historical. The Popocatépetl olivines from the different stages have distinct Fo-Ni signatures (Straub & Martin-Del Pozzo, 2001; Straub *et al.*, 2011) and also olivine CaO + Cr-spinel characteristics (Figure 10h), which identifies them as distinct, non-cogenetic mafic melt batches that are fed into the Popocatépetl system. There is no unidirectional temporal trend, and if there was once a fertile mantle, its products are either eroded or buried under younger series. How can mafic melts be produced from a longterm depleted mantle? We propose that mantle melting beneath Popocatépetl may have been sustained by a network of many fusible lithologies in the mantle, which may have been constructed by the continuous slab flux. Upon melting, individual mafic melts are extracted from certain parts of the network, until the larger mantle domain becomes too refractory and volcanism halts until sufficiently new fertile mantle has been advected by corner-flow which may cause volcanic activity to resume. This model is consistent with the many cycles of renewed volcanic activity Popocatépetl, that can be linked to the ascent of new mafic mantle melts (Straub & Martin-Del Pozzo, 2001; Mangler *et al.*, 2020).

Serial melting and global arc magma genesis

The observed olivine+Cr-spinel systematics are not unique to the TMVB, but align with similar data from high-Mg# magmas in the southernmost Cascades (Clynne & Borg, 1997), from Ruapehu volcano in the Taupo Volcanic Zone (Conway *et al.*, 2020) and from the Payenia backarc in the Andes Southern Volcanic Zone (Søager *et al.*, 2015; Brandt *et al.*, 2017). Thus, the serial melting may be common in arcs. In this context, several points emerge that are relevant for global arcs:

First, the serial melting model implies the *in-situ* depletion of the mantle wedge by active arc volcanism itself. This inference contrasts with studies that propose that the depleted arc front mantle may be residual to melting in the back-arc or rear-arc region from where it is dragged beneath the arc front by corner flow (e.g. Stolper & Newman, 1994; Hochstaedter *et al.*, 1996; Hochstaedter *et al.*, 2000; Ryan & Chauvel, 2014). It has also been proposed, that slab flux drives variations in the extent of melting, which would result to a variably depleted mantle wedge along the arc front (e.g. Kelley *et al.*, 2010; Barker *et al.*, 2020). This model is to some degree at variance with serial melting model that emphasizes that the frequency of melt extraction from the mantle as important factor in residual mantle evolution.

Secondly, the question arises how the melt CaO variations induced by serial melting relate to the robust CaO systematics

in global mafic arc magmas (Plank & Langmuir, 1988; Turner & Langmuir, 2015). At the global scale, melt CaO in high-Mg# ~55–65 arc magmas in thin-crusted oceanic arcs is similar high as in MORB, and both are higher by a factor of 3 than the low-CaO high-Mg# magmas from thick-crusted continental arcs (Figure 12). The difference has been linked to the extent of melting, which was inferred to be higher in oceanic than in continental arc settings (Plank & Langmuir, 1988; Turner & Langmuir, 2022). The high-Mg# TMVB magmas have end member character in the global array, which is confirmed by the low bulk rock CaO of high-Mg# samples studied (Figure 12). Nevertheless, the melt CaO range within the TMVB still varies by almost a factor of two between ~9.9 wt % and ~ ≤ 5.5 wt % CaO in calc-alkaline arc front magmas, which corresponds to about half of the global range (Figure 12). Thus, while serial melting does not upset the global systematics, it clearly creates considerable regional variations within in the TMVB.

Lastly, our study predicts that high-CaO oceanic arcs (e.g. Mariana, Izu Bonin, Tonga, Kermadec) should have high-CaO olivines that resemble MORB olivines. High CaO olivines with ~0.31 wt % and ~ 0.4 to 0.5 wt % CaO, respectively, have been indeed reported from Northwest Rota Seamount in the northern Mariana arcs (Tamura *et al.*, 2011) and from picrites in the Solomon arc (Kamenetsky *et al.*, 2006). However, at both locations, the high-CaO olivines are only part of a larger olivine population with variable CaO contents, that also includes lower CaO olivines (0.14 wt % and less) at high olivine Fo ≥ 86. Here, combined olivine CaO + Cr-spinel systematics could test whether the existence of the low CaO olivines in oceanic arcs conform to the CaO + Cr-spinel systematic of continental arcs and likewise may record the slab-flux driven serial melting in oceanic arc volcanoes.

CONCLUSIONS

The following are the conclusions of this study:

- Forsteritic olivines and their Cr-spinel inclusions from high-Mg# TMVB magmas preserve signatures of primary mantle melts.
- Rear-arc and arc-front olivine+Cr-spinels have different olivine CaO and Cr-spinel Cr# signatures, owing to their origin from mantle that is not (rear-arc) or strongly (arc-front) modified by the slab flux.
- The CaO contents of the olivines is principally controlled by the melt CaO of high-Mg# primitive TMVB magmas; other influences (melt H_2O, Fe) are minor.
- Olivine CaO + Cr-spinel Cr# systematics indicate in-situ source depletion of the arc front mantle by slab-flux driven serial melting.
- The regional arc-scale variations in melt CaO recorded by olivine CaO -Cr-spinel Cr# systematics record are superimposed on underlying global variations.

DATA AVAILABILITY

All new analytical data, together with a compilation of previously published bulk rock data and sample locations, are provided in Supplementary Appendix Tables 1 to 7, which are available at https://doi.org/10.6084/m9.figshare.22274359.v1.

Supplementary Data

Supplementary data are available at *Journal of Petrology* online.

Acknowledgements

Ofélia Pérez-Arvizu, Liliana Corona and Collin Kelso are thanked for lab support. The paper benefitted from the reviews by Maja Bar Rasmussen and two anonymous reviewers. Tod Waight is thanked for editorial handling. This study was financially supported by the U.S. National Science Foundation (grants EAR-19-21624 and -21643 to SMS and EW). Participation of V. Batanova and A. Sobolev and functioning of EPMA facility in ISTerre were supported by the grant from the European Research Council (ERC) under the European Union's Horizon H2020 research and innovation program (Synergy Grant MEET, grant agreement no.856555).

References

Agustín-Flores, J., Siebe, C. & Guilbaud, M. N. (2011). Geology and geochemistry of Pelagatos, Cerro del Agua, and dos Cerros monogenetic volcanoes in the sierra Chichinautzin volcanic field, south of México City. *Journal of Volcanology and Geothermal Research* **201**, 143–162. https://doi.org/10.1016/j.jvolgeores.2010.08.010.

Ahmadi, J., Widom, E., Straub, S. M., Sanchez, R., Kuentz, D., Gómez-Tuena, A., Espinasa-Perena, R., Bindeman, I. N. & Stuart, F. M. (2023) Testing Source vs. In: *Crustal Processing in High-Mg# Arc Magmas from the Trans-Mexican Volcanic Belt: Os Isotope Systematics in Olivine. Celebrating the 80th anniversary of Parícutin volcano*. Morelia, Mexico.

Ammannati, E., Jacob, D. E., Avanzinelli, R., Foley, S. F. & Conticelli, S. (2016). Low Ni olivine in silica-undersaturated ultrapotassic igneous rocks as evidence for carbonate metasomatism in the mantle. *Earth and Planetary Science Letters* **444**, 64–74. https://doi.org/10.1016/j.epsl.2016.03.039.

Arai, S. (1994). Compositional variation of olivine-chromian spinel in mg-rich magmas a guide to their residual peridotites. *Journal of Volcanology and Geothermal Research* **59**, 279–293. https://doi.org/10.1016/0377-0273(94)90083-3.

Ballentine, C. J. & Burnard, P. G. (2002). Production, release and transport of Noble gases in the continental crust. *Reviews in Mineralogy and Geochemistry* **47**, 481–538. https://doi.org/10.2138/rmg.2002.47.12.

Barker, S. J., Rowe, M. C., Wilson, C. J. N., Gamble, J. A., Rooyakkers, S. M., Wysoczanski, R. J., Illsley-Kemp, F. & Kenworthy, C. C. (2020). What lies beneath? Reconstructing the primitive magmas fueling voluminous silicic volcanism using olivine-hosted melt inclusions. *Geology* **48**, 504–508. https://doi.org/10.1130/G47422.1.

Beattie, P., Ford, C. & Russell, D. (1991). Partition coefficients for olivine-melt and orthopyroxene-melt systems. *Contributions to Mineralogy and Petrology* **109**, 212–224. https://doi.org/10.1007/BF00306480.

Bindeman, I. N., Ionov, D. A., Tollan, P. M. E. & Golovin, A. V. (2022). Oxygen isotope (δ18O, Δ'17O) insights into continental mantle evolution since the Archean. *Nature Communications* **13**, 3779. https://doi.org/10.1038/s41467-022-31586-9.

Birner, S. K., Warren, J. M., Cottrell, E., Davis, F. A., Kelley, K. A. & Falloon, T. J. (2017). Forearc Peridotites from Tonga record heterogeneous oxidation of the mantle following Subduction initiation. *Journal of Petrology* **58**, 1755–1780. https://doi.org/10.1093/petrology/egx072.

Bizimis, M., Salters, V. J. M. & Bonatti, E. (2000). Trace and REE content of clinopyroxenes from supra-subduction zone peridotites. Implications for melting and enrichment processes in island arcs. *Chemical Geology* **165**, 67–85. https://doi.org/10.1016/S0009-2541(99)00164-3.

Blatter, D. L. & Carmichael, I. S. E. (2001). Hydrous phases equilibria of a Mexican high-silica andesite: a candidate for a mantle origin? *Geology* **65**, 4043–4065. https://doi.org/10.1016/S0016-7037(01)00708-6.

Blatter, D. L., Sisson, T. W. & Hankins, W. B. (2013). Crystallization of oxidized, moderately hydrous arc basalt at mid-to lower-crustal pressures: implications for andesite genesis. *Contributions to Mineralogy and Petrology* **166**, 861–886. https://doi.org/10.1007/s00410-013-0920-3.

Brandt, F. E., Holm, P. M. & Søager, N. (2017). South-to-north pyroxenite–peridotite source variation correlated with an OIB-type to arc-type enrichment of magmas from the Payenia backarc of the Andean southern volcanic zone (SVZ). *Contributions to Mineralogy and Petrology* **172**, 1. https://doi.org/10.1007/s00410-016-1318-9.

Bryant, J. A., Yogodzinksi, G. M. & Churikova, T. G. (2011). High-mg# andesitic lavas of the Shisheisky complex, northern Kamchatka: implications for primitive calc-alkaline magmatism. *Contributions to Mineralogy and Petrology* **161**, 791–810. https://doi.org/10.1007/s00410-010-0565-4.

Cadoux, A., Missenard, Y., Martinez-Serrano, R. G. & Guillou, H. (2011). Trenchward Plio-quaternary volcanism migration in the trans-Mexican Volcanic Belt: the case of the Sierra Nevada range. *Geological Magazine* **148**, 492–506. https://doi.org/10.1017/S0016756810000993.

Cai, Y., LaGatta, A., Goldstein, S. L., Langmuir, C. H., Gomez-Tuena, A., Martin del Pozzo, A. L. & Carrasco-Nunez, G. (2014). Hafnium isotope evidence for slab melt contributions in hot slab arcs: an example of the central Mexican Volcanic Belt. *Chemical Geology* **377**, 45–55. https://doi.org/10.1016/j.chemgeo.2014.04.002.

Cavazos-Tovar, J. G., Gómez-Tuena, A. & Parolari, M. (2020). The origin and evolution of the Mexican cordillera as registered in modern detrital zircons. *Gondwana Research* **86**, 83–103. https://doi.org/10.1016/j.gr.2020.06.001.

Cervantes, P. & Wallace, P. J. (2003a). The role of H2O in subduction zone magmatism: new insights from melt inclusions in high-mg basalts from Central Mexico. *Geology* **31**, 235–238. https://doi.org/10.1130/0091-7613(2003)031<0235:ROHOIS=2.0.CO;2.

Cervantes, P. & Wallace, P. J. (2003b). Magma degassing and basaltic eruption styles: a case study of V2000 year BP Xitle volcano in Central Mexico. *Journal of Volcanology and Geothermal Research* **120**, 249–270. https://doi.org/10.1016/S0377-0273(02)00401-8.

Clynne, M. A. & Borg, L. E. (1997). Olivine and chromian spinel in primitive calc-alkaline and tholeiitic lavas from the southernmost Cascade Range, California: a reflection of relative fertility of the source. *The Canadian Mineralogist* **35**, 453–472.

Conway, C. E., Chamberlain, K. J., Harigane, Y., Morgan, D. J. & Wilson, C. J. N. (2020). Rapid assembly of high-mg andesites and dacites by magma mixing at a continental arc stratovolcano. *Geology* **48**, 1033–1037. https://doi.org/10.1130/G47614.1.

Coogan, L. A., Saunders, A. D. & Wilson, R. N. (2014). Aluminum-in-olivine thermometry of primitive basalts: evidence of an anomalously hot mantle source for large igneous provinces. *Chemical Geology* **368**, 1–10. https://doi.org/10.1016/j.chemgeo.2014.01.004.

De Hoog, J. C. M., Gall, L. & Cornell, D. H. (2010). Trace-element geochemistry of mantle olivine and application to mantle petrogenesis and geothermobarometry. *Chemical Geology* **270**, 196–215. https://doi.org/10.1016/j.chemgeo.2009.11.017.

Díaz-Bravo, B. A., Gómez-Tuena, A., Ortega-Obregón, C. & Pérez-Arvizu, O. (2014). The origin of intraplate magmatism in the western trans-Mexican Volcanic Belt. *Geophere* **10**, 340–373. https://doi.org/10.1130/GES00976.1.

Dick, H. J. B. & Bullen, T. (1984). Chromian spinel as a petrogenetic indicator in abyssal and alpine-type peridotites and spatially associated lavas. *Contributions to Mineralogy and Petrology* **86**, 54–76. https://doi.org/10.1007/BF00373711.

Eichelberger, J. C. (1978). Andesitic volcanism and crustal evolution. *Nature* **275**, 21–27. https://doi.org/10.1038/275021a0.

Elliott, T., Plank, T., Zindler, A., White, W. & Bourdon, B. (1997). Element transport from subducted slab to juvenile crust at the Mariana arc. *Journal of Geophysical Research* **102**, 14991–15019. https://doi.org/10.1029/97JB00788.

Feig, S. T., Koepke, J. & Snow, J. E. (2006). Effect of water on tholeiitic basalt phase equilibria: an experimental study under oxidizing conditions. *Contributions to Mineralogy and Petrology* **152**, 611–638. https://doi.org/10.1007/s00410-006-0123-2.

Ficini, E., Dal Zilio, L., Doglioni, C. & Gerya, T. V. (2017). Horizontal mantle flow controls subduction dynamics. *Scientific Reports* **7**, 7550. https://doi.org/10.1038/s41598-017-06551-y.

Gale, A., Dalton, C. A., Langmuir, C. H., Su, Y. & Schilling, J. G. (2013). The mean composition of ocean ridge basalts. *Geochemistry, Geophysics, Geosystems* **14**, 489–518. https://doi.org/10.1029/2012GC004334.

Gamal El Dien, H., Arai, S., Doucet, L.-S., Li, Z.-X., Kil, Y., Fougerouse, D., Reddy, S. M., Saxey, D. W. & Hamdy, M. (2019). Cr-spinel records metasomatism not petrogenesis of mantle rocks. *Nature Communications* **10**, 5103. https://doi.org/10.1038/s41467-019-13117-1.

Gavrilenko, M., Herzberg, C., Vidito, C., Carr, M. J., Tenner, T. & Ozerov, A. (2016). A calcium-in-olivine Geohygrometer and its application to Subduction zone Magmatism. *Journal of Petrology* **57**, 1811–1832. https://doi.org/10.1093/petrology/egw062.

GeoROC (2023). *Geochemistry of Rocks of the Oceans and Continents*. Georg-August Universitaet Goettingen. https://georoc.eu/.

Gleeson, M. L. M. & Gibson, S. A. (2019). Crustal controls on apparent mantle pyroxenite signals in ocean-island basalts. *Geology* **47**, 321–324. https://doi.org/10.1130/G45759.1.

Gómez-Tuena, A., Langmuir, C. H., Goldstein, S. L., Straub, S. M. & Ortega-Gutierrez, F. (2007). Geochemical evidence for slab melting in the trans-Mexican Volcanic Belt. *Journal of Petrology* **48**, 537–562. https://doi.org/10.1093/petrology/egl071.

Gómez-Tuena, A., Orozco-Esquivel, M. T. & Ferrari, L. (2007) Igneous petrogenesis of the Trans-Mexican Volcanic Belt. In: Alaniz-Álvarez S. A. & Nieto-Samaniego Á. F. (eds) *Geology of Mexico: Celebrating the Centenary of the Geological Society of Me'xico*, Geological Society of America, Special Paper 422 Boulder, Colorado, pp.129–181.

Gómez-Tuena, A., Díaz-Bravo, B., Vázquez-Duarte, A., Pérez-Arvizu, O. & Laura Mori, L. (2014) Andesite petrogenesis by slab-derived plume pollution of a continental rift. In: Gomez-Tuena A., Straub S. M. & Zellmer G. F. (eds) *Orogenic Andesite and Crustal Growth*, Vol. **385**. London: Geol Soc London Spec Pub, pp.65–101.

Gómez-Tuena, A., Cavazos-Tovar, J. G., Parolari, M., Straub, S. M. & Espinasa-Pereña, R. (2018a). Geochronological and geochemical evidence of continental crust 'relamination' in the origin of intermediate arc magmas. *Lithos* **322**, 52–66. https://doi.org/10.1016/j.lithos.2018.10.005.

Gómez-Tuena, A., Mori, L. & Straub, S. M. (2018b). Geochemical and petrological insights into the tectonic origin of the trans-Mexican Volcanic Belt. *Earth Science Reviews* **183**, 153–181. https://doi.org/10.1016/j.earscirev.2016.12.006.

Graham, D. W. (2002). Noble gas isotope geochemistry of Mid-Ocean ridge and Ocean Island basalts: characterization of mantle source reservoirs. *Reviews in Mineralogy and Geochemistry* **47**, 247–317. https://doi.org/10.2138/rmg.2002.47.8.

Herzberg, C. (2006). Petrology and thermal structure of the Hawaiian plume from Mauna kea. *Nature* **444**, 605–609. https://doi.org/10.1038/nature05254.

Hess, P. C. (1994) Phase equilibria constraints on the origin of ocean floor basalts. In: Morgan J. P., Blackman D. K. & Sinton J. M. (eds) *Mantle Flow and Melt Generation at Mid-Ocean*. Ridges: American Geophysical Union, pp.67–102.

Hochstaedter, A. G., Kepezhinskas, P., Defant, M., Drummond, M. & Koloskov, A. (1996). Insights into the volcanic arc mantle wedge from magnesian lavas from the Kamchatka arc. *Journal of Geophysical Research* **101**, 697–712. https://doi.org/10.1029/95JB02404.

Hochstaedter, A. F., Gill, J. B., Taylor, B., Ishizuka, O., Yuasa, M. & Morita, S. (2000). Across-arc geochemical trends in the Izu-Bonin arc: constraints on source composition and mantle melting. *Journal of Geophysical Research* **105**, 495–512. https://doi.org/10.1029/1999JB900125.

Johnson, E. R., Wallace, P. J., Delgado-Granados, H., Manea, V. C., Kent, A. J. R., Bindeman, I. N. & Donegan, C. S. (2009). Subduction-related volatile recycling and magma generation beneath Central Mexico: insights from melt inclusions, oxygen isotopes and geodynamic models. *Journal of Petrology* **50**, 1729–1764. https://doi.org/10.1093/petrology/egp051.

Jurewicz, A. J. G. & Watson, E. B. (1988). Cations in olivine, part 1: calcium partitioning and calcium-magnesium distribution between olivines and coexisting melts, with petrologic applications. *Contributions to Mineralogy and Petrology* **99**, 176–185. https://doi.org/10.1007/BF00371459.

Kamenetsky, V. S., Crawford, A. J. & Meffre, S. (2001). Factors controlling chemistry of magmatic spinel: an empirical study of associated olivine, Cr-spinel and melt inclusions from primitive rocks. *Journal of Petrology* **42**, 655–671. https://doi.org/10.1093/petrology/42.4.655.

Kamenetsky, V. S., Elburg, M., Arculus, R. & Thomas, R. (2006). Magmatic origin of low-Ca olivine in subduction-related magmas: co-existence of contrasting magmas. *Chemical Geology* **233**, 346–357. https://doi.org/10.1016/j.chemgeo.2006.03.010.

Kelley, K. A. & Cottrell, E. (2009). Water and the oxidation state of Subduction zone magmas. *Science* **325**, 605–6607. https://doi.org/10.1126/science.1174156.

Kelley, K. A., Plank, T., Newman, S., Stolper, E., Grove, T. L., Parman, S. W. & Hauri, E. H. (2010). Mantle melting as a function of water content beneath the Mariana arc. *Journal of Petrology* **51**, 1711–1738. https://doi.org/10.1093/petrology/egq036.

Kent, A. J. R., Darr, C., Koleszar, A. M., Salisbury, M. J. & Cooper, K. M. (2010). Preferential eruption of andesitic magmas through recharge filtering. *Nature Geoscience* **3**, 631–636. https://doi.org/10.1038/ngeo924.

Kushiro, I. (2001). Partial melting experiments on Peridotite and origin of Mid-Ocean ridge basalt. *Annual Review of Earth and Planetary Sciences* **29**, 71–107. https://doi.org/10.1146/annurev.earth.29.1.71.

LaGatta, A. B. (2003) Arc magma genesis in the Eastern Mexican Volcanic Belt. In: *Department of Earth and Environmental Sciences*. New York: Columbia University, p.329.

Lages, J., Rizzo, A. L., Aiuppa, A., Samaniego, P., Le Pennec, J. L., Ceballos, J. A., Narváez, P. A., Moussallam, Y., Bani, P., Schipper, C. I., Hidalgo, S., Gaglio, V., Alberti, E. & Sandoval-Velasquez, A. (2021). Noble gas magmatic signature of the Andean northern volcanic zone from fluid inclusions in minerals. *Chemical Geology* **559**, 119966. https://doi.org/10.1016/j.chemgeo.2020.119966.

Lange, R. A. & Carmichael, I. S. E. (1990). Hydrous basaltic Andesites associated with Minette and Related lavas in Western Mexico. *Journal of Petrology* **31**, 1225–1259. https://doi.org/10.1093/petrology/31.6.1225.

Langmuir, C. H., Klein, E. M. & Plank, T. (2013) Petrological Systematics of Mid-Ocean Ridge Basalts: Constraints on Melt Generation Beneath Ocean Ridges. In: Morgan J. P., Blackman D. K. & Sinton J. M. (eds) *Mantle Flow and Melt Generation at Mid-Ocean Ridges: Morgan/Mantle Flow and Melt Generation at Mid-Ocean Ridges*. Washington: American Geophysical Union, pp.183–280.

Larrea, P., Widom, E., Siebe, C., Salinas, S. & Kuentz, D. (2019). A re-interpretation of the petrogenesis of Paricutin volcano: distinguishing crustal contamination from mantle heterogeneity. *Chemical Geology* **504**, 66–82. https://doi.org/10.1016/j.chemgeo.2018.10.026.

Laubier, M., Grove, T. L. & Langmuir, C. H. (2014). Trace element mineral/melt partitioning for basaltic and basaltic andesitic melts: an experimental and laser ICP-MS study with application to the oxidation state of mantle source regions. *Earth and Planetary Science Letters* **392**, 265–278. https://doi.org/10.1016/j.epsl.2014.01.053.

Leeman, W. P. & Smith, D. J. (2018). The role of magma mixing, identification of mafic magma inputs, and structure of the underlying magmatic system at Mount St. Helens. *American Mineralogist* **103**, 1925–1944. https://doi.org/10.2138/am-2018-6555.

Libourel, G. (1999). Systematics of calcium partitioning between olivine and silicate melt: implication for melt structure and calcium content of magmatic olivine. *Contributions to Mineralogy and Petrology* **136**, 63–80. https://doi.org/10.1007/s004100050524.

Luhr, J. F. (1997). Extensional tectonics and the diverse primitive volcanic rocks in the western Mexican Volcanic Belt. *The Canadian Mineralogist* **35**, 473–500.

Luhr, J. E., James, F. A., Carmichael, I. S. E., Nelson, S. A. & Hasenaka, T. (1989). Primitive calc-alkaline and alkaline rock types from the Western Mexican Volcanic Belt. *Journal of Geophysical Research* **94**, 4515–4530. https://doi.org/10.1029/JB094iB04p04515.

Ma, S. & Shaw, C. S. J. (2021). An experimental study of trace element partitioning between Peridotite minerals and alkaline basaltic melts at 1250°C and 1 GPa: crystal and melt composition impacts on partition coefficients. *Journal of Petrology* **62**. https://doi.org/10.1093/petrology/egab084.

Mangler, M. F., Petrone, C. M., Hill, S., Delgado-Granados, H. & Prytulak, J. (2020). A Pyroxenic view on magma hybridization and crystallization at Popocatépetl volcano, Mexico. *Frontiers in Earth Science* **8**. https://doi.org/10.3389/feart.2020.00362.

Matzen, A. K., Baker, M. B., Beckett, J. R. & Stolper, E. M. (2013). The temperature and pressure dependence of nickel partitioning between olivine and silicate melt. *Journal of Petrology* **54**, 2521–2545. https://doi.org/10.1093/petrology/egt055.

Matzen, A. K., Wood, B. J., Baker, M. B. & Stolper, E. M. (2017). The roles of pyroxenite and peridotite in the mantle sources of oceanic basalts. *Nature Geoscience* **10**, 530–535. https://doi.org/10.1038/ngeo2968.

Maurel, C. & Maurel, P. (1982). Etude experimentale de l'equilibire Fe2+-Fe3+ dans les spinelles chromiferes et les liquides silicates basiques, a 1 atm. *C R Acad Sc Paris t 295, Serie II* , 209–212.

Mesa, J. & Lange, R. A. (2021). Origin of alkali olivine basalts and hawaiites in the western Mexican arc: evidence of rapid phenocryst growth and magma mixing during ascent along fractures. *Geosphere* **17**, 1563–1588. https://doi.org/10.1130/GES02365.1.

Moore, G. & Carmichael, I. S. E. (1998). The hydrous phase equilibria (to 3 kbar) of an andesite and basaltic andesite from western Mexico: constraints on water content and conditions of phenocryst growth. *Contributions to Mineralogy and Petrology* **130**, 304–319. https://doi.org/10.1007/s004100050367.

Muentener, O. & Ulmer, P. (2018). Arc crust formation and differentiation constrained by experimental petrology. *American Journal of Science* **318**, 64–89. https://doi.org/10.2475/01.2018.04.

Nekrylov, N., Portnyagin, M. V., Kamenetsky, V. S., Mironov, N. M., Churikova, T. G., Plechov, P. Y., Abersteiner, A., Gorbach, N. V., Gordeychik, B. N., Krasheninnikov, S. P., Tobelko, D. P., Shur, M. Y., Tetroeva, S. A., Volynets, A. O., Hoernle, K. & Wörner, G. (2018). Chromium spinel in Late Quaternary volcanic rocks from Kamchatka: implications for spatial compositional variability of subarc mantle and its oxidation state. *Lithos* **322**, 212–224. https://doi.org/10.1016/j.lithos.2018.10.011.

Nixon, G. T. (1988). Petrology of the younger andesites and dacites of Iztaccihuatl volcano, Mexico: I. Disequilibrium phenocrysts assemblages as indicators of magma chamber processes. *Journal of Petrology* **29**, 213–264. https://doi.org/10.1093/petrology/29.2.213.

Ortega-Gutiérrez, F., Elías-Herrera, M. & Dávalos-Elizondo, M. G. (2008). On the nature and role of the lower crust in the volcanic front of the trans-Mexican Volcanic Belt and its fore-arc region, southern and Central Mexico. *Revista Mexicana de Ciencias Geologicas* **25**, 346–364.

Parkinson, I. J. & Pearce, J. A. (1998). Peridotites from the Izu-Bonin-Mariana Forearc (ODP leg 125): evidence for mantle melting and melt-mantle interaction in a supra-subduction zone setting. *Journal of Petrology* **39**, 1577–1618. https://doi.org/10.1093/petroj/39.9.1577.

Parman, S. & Grove, T. (2004). Harzburgite melting with and without H2O: experimental data and predictive modeling. *Journal of Geophysical Research* **109**, B02201. https://doi.org/10.1029/2003JB002566.

Parolari, M., Gómez-Tuena, A., Cavazos-Tovar, J. G. & Hernández-Quevedo, G. (2018). A balancing act of crust creation and destruction along the western Mexican convergent margin. *Geology* **46**, 455–458. https://doi.org/10.1130/G39972.1.

Parolari, M., Gómez-Tuena, A., Errázuriz-Henao, C. & Cavazos-Tovar, J. G. (2021). Orogenic andesites and their link to the continental rock cycle. *Lithos* **382-383**, 105958. https://doi.org/10.1016/j.lithos.2020.105958.

Pearce, J. A. & Arculus, R. J. (2021) Boninites. In: Alderton D. & Elias S. A. (eds) *Encyclopedia of Geology*, Second edn. Oxford: Elsevier, pp.113–129.

Pearce, J. A. & Reagan, M. K. (2019). Identification, classification, and interpretation of boninites from Anthropocene to Eoarchean using Si-mg-Ti systematics. *Geosphere* **15**, 1008–1037. https://doi.org/10.1130/GES01661.1.

Pearce, J. A., Barker, P. F., Edwards, S. J., Parkinson, I. J. & Leat, P. T. (2000). Geochemistry and tectonic significance of peridotites from the South Sandwich arc-basin system, South Atlantic. *Contributions to Mineralogy and Petrology* **139**, 36–53. https://doi.org/10.1007/s004100050572.

Plank, T. & Langmuir, C. H. (1988). An evaluation of the global variations in the major element chemistry of arc basalts. *Earth and Planetary Science Letters* **90**, 349–370. https://doi.org/10.1016/0012-821X(88)90135-5.

Putirka, K. D. (2008). Thermometers and barometers for volcanic systems. *Reviews in Mineralogy and Geochemistry* **69**, 61–120. https://doi.org/10.2138/rmg.2008.69.3.

Rasmussen, M. B., Halldórsson, S. A., Gibson, S. A. & Guðfinnsson, G. H. (2020). Olivine chemistry reveals compositional source heterogeneities within a tilted mantle plume beneath Iceland. *Earth and Planetary Science Letters* **531**, 116008. https://doi.org/10.1016/j.epsl.2019.116008.

Roberge, J., Delgado-Granados, H. & Wallace, P. J. (2009). Mafic magma recharge supplies high CO2 and SO2 gas fluxes from Popocatépetl volcano, Mexico. *Geology* **37**, 107–110. https://doi.org/10.1130/G25242A.1.

Roeder, P. E. & Emslie, R. F. (1970). Olivine-liquid equilibrium. *Contributions to Mineralogy and Petrology* **29**, 275–289. https://doi.org/10.1007/BF00371276.

Ryan, J. G. & Chauvel, C. (2014) 3.13 - The Subduction-Zone Filter and the Impact of Recycled Materials on the Evolution of the Mantle. In: Holland H. D. & Turekian K. K. (eds) *Treatise on Geochemistry*, Second edn. Oxford: Elsevier, pp.479–508.

Sandoval-Velasquez, A., Rizzo, A. L., Frezzotti, M. L., Saucedo, R. & Aiuppa, A. (2021). The composition of fluids stored in the central Mexican lithospheric mantle: inferences from noble gases and CO2 in mantle xenoliths. *Chemical Geology* **576**, 120270. https://doi.org/10.1016/j.chemgeo.2021.120270.

Sas, M., Debari, S. M., Clynne, M. A. & Rusk, B. G. (2017). Using mineral geochemistry to decipher slab, mantle, and crustal input in the generation of high-mg andesites and basaltic andesites from the northern Cascade arc. *American Mineralogist* **102**, 948–965.

Schaaf, P., Stimac, J., Siebe, C. & Macias, J. L. (2005). Geochemical evidence for mantle origin and crustal processes in volcanic rocks from Popocatepetl and surrounding monogenetic volcanoes, Central Mexico. *Journal of Petrology* **46**, 1243–1282. https://doi.org/10.1093/petrology/egi015.

Siebe, C., Rodriguez-Lara, V., Schaaf, P. & Abrams, M. (2004a). Geochemistry, Sr-Nd isotope composition, and tectonic setting of Holocene Pelado, Guespalapa and Chichinautzin scoria cones, south of Mexico City. *Journal of Volcanology and Geothermal Research* **130**, 197–226. https://doi.org/10.1016/S0377-0273(03)00289-0.

Siebe, C., Rodriguez-Lara, V., Schaaf, P. & Abrams, M. (2004b). Radiocarbon ages of Holocene Pelado, Guespalapa, and Chichinautzin scoria cones, south of Mexico City: implications for archeology and future hazards. *Bulletin of Volcanology* **66**, 203–225. https://doi.org/10.1007/s00445-003-0304-z.

Siebe, C., Arana-Salinas, L. & Abrams, M. (2005). Geology and radiocarbon ages of Tlaloc, Tlacotenco, Cuauhtzin, Hijo del Cuauhtzin, Teuhtli, and Ocusacayo monogenetic volcanoes in the central part of the sierra Chichinautzin, Mexico. *Journal of Volcanology and Geothermal Research* **141**, 225–243. https://doi.org/10.1016/j.jvolgeores.2004.10.009.

Søager, N., Portnyagin, M., Hoernle, K., Holm, P. M., Hauff, F. & Garbe-Schoenberg, D. (2015). Olivine major and trace element compositions in southern Payenia basalts, Argentina: evidence for Pyroxenite-Peridotite melt mixing in a Back-arc setting. *Journal of Petrology* **56**, 1495–1518. https://doi.org/10.1093/petrology/egv043.

Sobolev, A. V., Hofmann, A. W., Sobolev, V. S. & Nikogosian, I. K. (2005). An olivine-free mantle source of Hawaiian shield basalts. *Nature* **434**, 590–597. https://doi.org/10.1038/nature03411.

Sobolev, A. V., Hofmann, A. W., Kuzmin, D. V., Yaxley, G. M., Arndt, N. T., Chung, S. L., Danyushevsky, L. V., Elliott, T., Frey, F. A., Garcia, M. O., Gurenko, A. A., Kamenetsky, V. S., Kerr, A. C., Krivolutskaya, N. A., Matvienkov, V. K., Nikogosian, I. K., Rocholl, A., Sigurdsson, I. A., Sushchevkaya, N. M. & Teklay, M. (2007). The amount of recycled crust in sources of mantle-derived melts. *Science* **316**, 412–417. https://doi.org/10.1126/science.1138113.

Stolper, E. & Newman, S. (1994). The role of water in the petrogenesis of Mariana trough magmas. *Earth and Planetary Science Letters* **121**, 293–325. https://doi.org/10.1016/0012-821X(94)90074-4.

Straub, S. M. (2019). Compilation of published major and trace elements and Sr-Nd-Pb-Hf isotope ratios of quaternary-age arc

volcanic rocks from the trans-Mexican Volcanic Belt. *EarthChem Library* . https://doi.org/10.1594/IEDA/100665.

Straub, S. M. & Martin-Del Pozzo, A. L. (2001). The significance of phenocryst diversity in tephra from recent eruptions at Popocatepetl volcano (Central Mexico). *Contributions to Mineralogy and Petrology* **140**, 487–510. https://doi.org/10.1007/PL00007675.

Straub, S. M., LaGatta, A. B., Martin-Del Pozzo, A. L. & Langmuir, C. H. (2008). Evidence from high Ni olivines for a hybridized peridotite/pyroxenite source for orogenic andesites from the central Mexican Volcanic Belt. *Geochem Geophys Geosys* **9**, Q03007. https://doi.org/10.1029/2007GC001583.

Straub, S. M., Gomez-Tuena, A., Stuart, F. M., Zellmer, G. F., Espinasa-Perena, R., Cai, M. Y. & Iizuka, Y. (2011). Formation of hybrid arc andesites beneath thick continental crust. *Earth and Planetary Science Letters* **303**, 337–347. https://doi.org/10.1016/j.epsl.2011.01.013.

Straub, S. M., Gomez-Tuena, A., Zellmer, G. F., Espinasa-Perena, R., Stuart, F. M., Cai, Y., Langmuir, C. H., Martin-Del Pozzo, A. & Mesko, G. T. (2013a). The processes of melt differentiation in arc volcanic rocks: insights from OIB-type arc magmas in the central Mexican Volcanic Belt. *Journal of Petrology* **54**, 665–701. https://doi.org/10.1093/petrology/egs081.

Straub, S. M., Gomez-Tuena, A., Zellmer, G. F., Espinasa-Perena, R., Stuart, F. M., Cai, Y., Langmuir, C. H., Martin-Del Pozzo, A. & Mesko, G. T. (2013b). The processes of melt differentiation in arc volcanic rock: insights from OIB-type arc magmas in the central Mexican Volcanic Belt: reply to a critical comment by Claus Siebe (2013). *Journal of Petrology* **54**, 1551–1554. https://doi.org/10.1093/petrology/egt021.

Straub, S. M., Zellmer, G. F., Gómez-Tuena, A., Espinasa-Perena, R., Martin-Del Pozzo, A. L., Stuart, F. M. & Langmuir, C. H. (2014) A genetic link between silicic slab components and calc-alkaline arc volcanism in central Mexico. In: Gomez-Tuena A., Straub S. M. & Zellmer G. F. (eds) *Orogenic Andesites and Crustal Growth Geol Soc London Spec Pub 385*. London: The Geological Society of London pp.31–64.

Straub, S. M., Gomez-Tuena, A., Bindeman, I. N., Bolge, L. L., Brandl, P. A., Espinasa-Perena, R., Solari, L., Stuart, F. M., Vannucchi, P. & Zellmer, G. F. (2015). Crustal recycling by Subduction erosion in the central Mexican Volcanic Belt. *Geology* **166**, 29–52.

Streck, J., Dungan, M. A., Malavassi, E., Reagan, M. K. & Bussy, F. (2002). The role of basalt replenishment in the generation of basaltic andesites of the ongoing activity at Arenal volcano, Costa Rica: evidence from clinopyroxene and spinel. *Bulletin of Volcanology* **64**, 316–327. https://doi.org/10.1007/s00445-002-0209-2.

Tamura, Y., Ishizuka, O., Stern, R. J., Shukuno, H., Kawabata, H., Embley, R. W., Hirahara, Y., Chang, Q., Kimura, J. I., Tatsumi, Y., Nunokawa, A. & Bloomer, S. H. (2011). Two primary basalt MagmaTypes from Northwest Rota-1 volcano, Mariana arc and its mantle Diapir or mantle wedge plume. *Journal of Petrology* **52**, 1143–1183. https://doi.org/10.1093/petrology/egr022.

Turner, S. J. & Langmuir, C. H. (2015). The global chemical systematics of arc front stratovolcanoes: evaluating the role of crustal processes. *Earth and Planetary Science Letters* **422**, 182–193. https://doi.org/10.1016/j.epsl.2015.03.056.

Turner, S. J. & Langmuir, C. H. (2022). An evaluation of five models of arc volcanism. *Journal of Petrology* **63**. https://doi.org/10.1093/petrology/egac010.

Turner, S. J., Langmuir, C. H., Dungan, M. A. & Escrig, S. (2017). The importance of mantle wedge heterogeneity to subduction zone magmatism and the origin of EM1. *Earth and Planetary Science Letters* **472**, 216–228. https://doi.org/10.1016/j.epsl.2017.04.051.

Wallace, P. J. & Carmichael, I. S. E. (1999). Quaternary volcanism near the valley of Mexico: implications for subduction zone magmatism and the effects of crustal thickness variations on primitive magma compositions. *Contributions to Mineralogy and Petrology* **135**, 291–314. https://doi.org/10.1007/s004100050513.

Wang, Z. & Gaetani, G. A. (2008). Partitioning of Ni between olivine and siliceous eclogite partial melt: experimental constraints on the mantle source of Hawaiian basalts. *Contributions to Mineralogy and Petrology* **156**, 661–678. https://doi.org/10.1007/s00410-008-0308-y.

Warren, J. M. (2016). Global variations in abyssal peridotite compositions. *Lithos* **248-251**, 193–219. https://doi.org/10.1016/j.lithos.2015.12.023.

Witt-Eickschen, G. & O'Neill, H. (2005). The effect of temperature on the equilibrium distribution of trace elements between clinopyroxene, orthopyroxene, olivine and spinel in upper mantle peridotite. *Chemical Geology* **221**, 65–101. https://doi.org/10.1016/j.chemgeo.2005.04.005.

Zamboni, D., Trela, J., Gazel, E., Sobolev, A. V., Cannatelli, C., Lucchi, F., Batanova, V. G. & De Vivo, D. (2017). New insights into the Aeolian Islands and other arc source compositions from high-precision olivine chemistry. *Lithos* **272-273**, 185–191. https://doi.org/10.1016/j.lithos.2016.12.004.